IEEE Access
Multidisciplinary ⋮ Rapid Review ⋮ Open Access Journal

Received May 25, 2020, accepted June 7, 2020. Date of publication xxxx 00, 0000, date of current version xxxx 00, 0000.

Digital Object Identifier 10.1109/ACCESS.2020.3003192

Non-Isolated High-Gain Triple Port DC–DC Buck-Boost Converter With Positive Output Voltage for Photovoltaic Application

AQ:1 **BALAJI CHANDRASEKAR[1], (Graduate Student Member, IEEE), CHELLAMMAL NALLAPERUMAL[1],**
AQ:2 **SANJEEVIKUMAR PADMANABAN[2], (Senior Member, IEEE),**
MAHAJAN SAGAR BHASKAR[3], (Member, IEEE), JENS BO HOLM-NIELSEN[2],
ZBIGNIEW LEONOWICZ[4], (Senior Member, IEEE), AND SAMSON O. MASEBINU[2,5]

[1]Department of Electrical and Electronics Engineering, SRM Institute of Science and Technology, Chennai 603203, India
[2]Center for Bioenergy and Green Engineering, Department of Energy Technology, Aalborg University, 6700 Esbjerg, Denmark
[3]Renewable Energy Lab, Department of Communications and Networks Engineering, College of Engineering, Prince Sultan University, Riyadh 11586, Saudi Arabia
[4]Faculty of Electrical Engineering, Wroclaw University of Science and Technology, 50370 Wroclaw, Poland
[5]Process Energy and Environmental Technology Station (PEETS), Faculty of Engineering and the Built Environment, University of Johannesburg, Doornfontein Campus, Johannesburg 2028, South Africa

Corresponding authors: Balaji Chandrasekar (balajic@srmist.edu.in) and Sanjeevikumar Padmanaban (san@et.aau.dk)

AQ:3 This work was supported by the Danida Mobility Grant, responsible for the Ministry of Foreign Affairs of Denmark (MFA), Act 7 on Denmark's International Development Cooperationm, under Grant 19-MG04AAU.

AQ:4 **ABSTRACT** The solar PV based power generation systems are growing faster due to the depletion of fossil fuels and environmental concerns. Combining PV panels and energy buffers such as battery through multi-port converter is one of the viable solutions to deal with the intermittency of PV power. The goal of this paper is to design and analyze the proposed triple port DC-DC buck-boost converter for high step-up/step-down applications. It has two unidirectional ports (port-1 and port-3) and one bi-directional port (port-2) for harnessing photovoltaic energy and charging the battery. At port-1, the combined structure of buck and buck-boost converter is used with a particular arrangement of switches and inductors. The step-up/step-down voltage conversion ratio is higher than the conventional buck-boost converter, and the polarity of the output voltage is maintained positive. The battery is added at the bi-directional port, for the storage of energy through the bi-directional boost converter. The switches operate synchronously for most of the modes making the control strategy simple. The characteristics and modes of operation along with a switching strategy, are elaborated. Experimental results are presented which validate the agreement with the developed theoretical expectation.

INDEX TERMS Buck-Boost converter, DC-DC, non-isolated, bi-directional, triple port, photovoltaic.

NOMENCLATURE

S_1, S_2, S_c, S_d	Switches
D_1, D_2, D_c, D_d	Diodes
L_1, L_2, L_3	Inductors
C_0, C_1	Capacitors
V_{PV}, V_{Bt}, V_o	Photovoltaic voltage, Battery voltage, Load voltage (Average values)
k_1, k_2, k_3	The duty cycle of state 1, 2, 3
$V_{S1}, V_{S2}, V_{Si}, V_{Sc}, V_{Sd}$	Voltage across switches
$\Delta i_{L1}, \Delta i_{L2}, \Delta i_{L3}$	Ripples in the current of inductor L_1, L_2, and L_3.
i_{L1}, i_{L2}, i_{L3}	inductor L_1, L_2, and L_3 currents
I_{L1}, I_{L2}, I_{L3}	Average inductor L_1, L_2, and L_3 currents
V_{C1}, V_{C0}	The average voltage across capacitor C_1 and C_0
v_{C1}, v_{C0}	The voltage across capacitor C_1 and C_0
$\Delta V_{C1}, \Delta VC_0$	Ripples voltage across capacitor C_1 and C_0.
R, T, f_s	Load, total time-period, switching frequency
i_{C1}, i_{C2}, i_{C0}	currents through capacitor C_1, C_2, C_0

The associate editor coordinating the review of this manuscript and approving it for publication was Feng Wu.

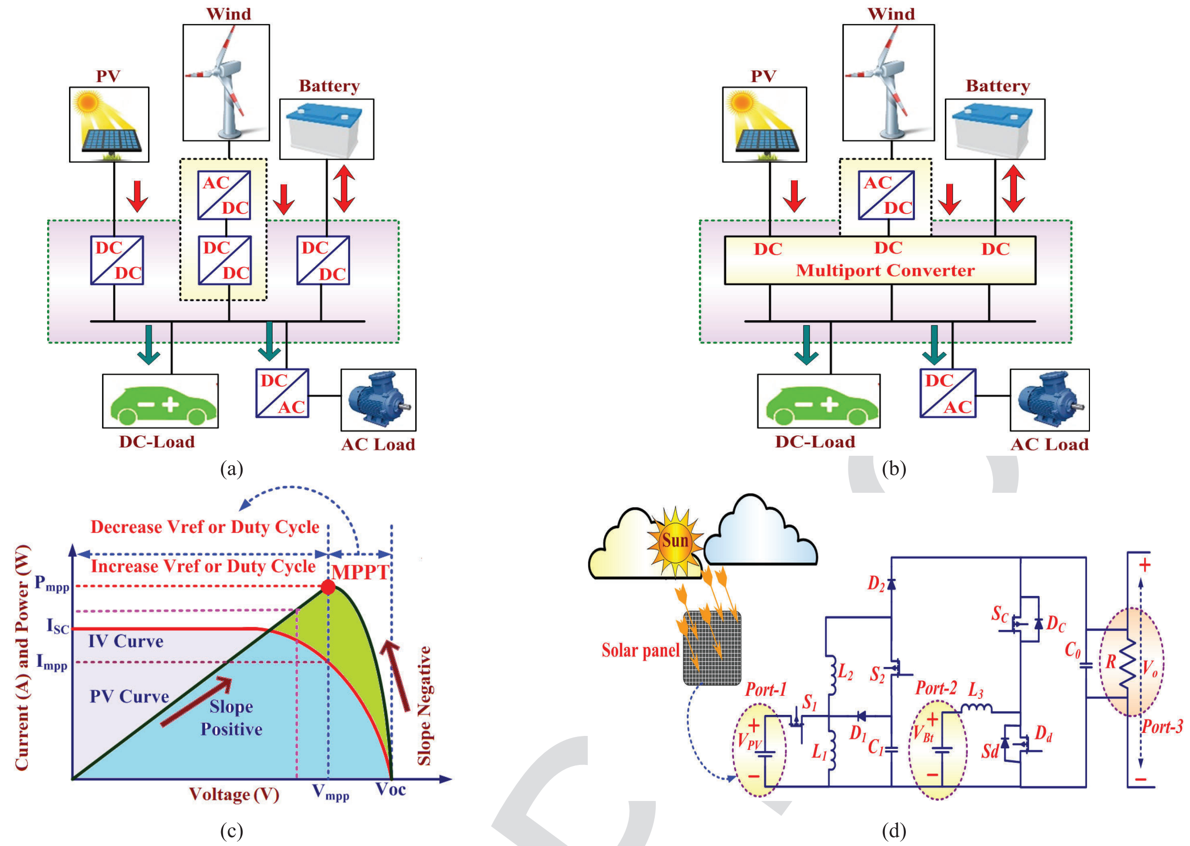

FIGURE 1. **Block Diagram, PV characteristics and Power Circuit (a) Structure of conventional converter based PV-Wind-Battery system, (b) Structure of multi-port converter based PV-Wind- Battery system, (c) Concept to track Maximum Power Point (MPP) using P-V and I-V characteristics, (d) Proposed triple port DC-DC buck-boost converter.**

I_{C1}, I_{C2}, I_{C0}	Average currents through capacitor C_1, C_2, C_0
k_{Sx}	The duty cycle of switch S_x
$\Delta i_{L(peak-peak)}$	Peak-to-peak inductor current variation
$x(t)$, $u(t)$	State vector and input vector
$V_{o(ref)}$	Reference of the load voltage
SOC	State of charge of the battery
$I_{Bt(ref)}$	The maximum discharge current of the battery
$I_{Bt(avg)}$	Regulated average battery current

I. INTRODUCTION

Presently the fossil fuels like coal, oil and natural gas are being depleted at a steady rate and soon cease to exist. Effects are immense pollution and detrimental to the environment. Consequently, extensive research is being carried out in the field of renewable energy resources and systems to find an environmentally free, cheap, efficient, and reliable solution [1]. Nevertheless, renewable energy resources are intermittent. As a result, multiple energy resources usage and their storage become necessary at the point of a power crisis scenario. However, the challenging task is the integration of multiple energy sources with different magnitude scales. Step-up and step-down voltage conversions are also mandatory with high efficiency for real-time applications due to the variation of voltage range in demand. The series/parallel combination of the photovoltaic (PV) panels is not a viable solution to increase the voltage/current due to the requirement of large space and cost [2]–[4]. Thus, the DC-DC converter with a high gain voltage conversion ratio is required to achieve high voltage outputs [5]. Several DC-DC converters are addressed and achieved high voltage by using several inductors and capacitors combinations with increased parasitic losses and bulky in size [6], [7]. Multi-port converters technologies are proven to utilize renewable energy resources efficiently. Also, it plays an essential role in charging/discharging of battery for real-time application. Fig. 1(a)-(b) elaborates the PV-Wind-Battery system using a conventional and multi-port converter, respectively. Recently, various multi-port converter topologies are addressed in the literature with postulated various rules for the effective designing of converters. In [8], sextuple output triad converter is proposed by utilizing switched inductor, boost, CUK and SEPIC configurations. Three unidirectional ports are powered from the single input port and using this sextupling converter loading is possible. In [9], four basic rules, assumptions, restrictions and conditions have been stated, to realize a multiple-input converter from its single input version with a minimum number of components and high feasibility. Using CUK and SEPIC, six new multi-port converter topologies are addressed. However, reliability is negatively affected as standard components and also acts as single points of failure for the entire converter. There is no bi-directional port (hence, charging and discharging operation is not possible). This converter also required a large number of semiconductor devices with a high voltage rating. In [10], the general approach was proposed to develop multi-input converters. Which supplies power from all the input sources to the load either individually or simultaneously without using coupled transformers. Extra Pulsating Voltage Sources (PVS) and Pulsating Current Source (PCS) are added in the PWM converter with suitable connection to derive new multiple-input converters (MIC). Quasi-MIC and Duplicated MIC structures are proposed by utilizing (PVS and PCS) in six PWM converter. Nonetheless, due to the absence of the bi-directional port, these topologies are not suitable for the battery-powered system. A new family of multi-input converters based on three switches leg introduced in [11]. Depending on the switching states, the converters have three modes of operations; buck, boost and inverter mode. However, the duty ratio is limited due to buck, and boost the operation of DC-DC conversion ports. Further, the complexity of the control circuit, the number of inductors and switches are increased as the number the ports increases.

A triple port high gain non-isolated DC-DC converter for PV application addressed by [12], which uses a coupled inductor technique to obtain high voltage gain. The solution to feeding PV energy to high voltage DC bus is achieved and suitable for multiple renewable energy sources due to its multiple input capability. However, this converter required a large number of semiconductor devices with the coupled inductor; which makes the circuit bulky and costly bulky circuit. In [13], a systematic method to derive a multi-port converter family (multi-input as well as multi-output) is proposed based on DC-Link Inductor (DLI) concept and buck-boost converter. These configurations are the prominent solution for renewable energy systems compared to conventional standard DC-bus based solution. Since the bulky DC-link, a capacitor is avoided. However, the number of switches increases and challenges are with the digital controller implementation. In [14], the design of a single switch non-isolated triple port converter for a stand-alone photovoltaic power system with energy storage is proposed. A synchronous switch with two diodes is used to replace two individual switches. Here, the challenging task is that the converters in both stages must work synchronously to have a single switching and only suitable for floating type loads. In [15], new single switch non-isolated transformer-less buck-boost DC-DC converter is proposed with low-voltage stress on the switch. The voltage gain is higher than the conventional boost, buck-boost, Cuk, SEPIC, and Zeta converters for a given duty cycle.

Nonetheless, no provision is present for the storage of excess energy and required a large number of diode, inductor, and capacitor. In [16], a set of basic rules for generating multi-input converters topologies are proposed. In particular, systematic synthesis of two multi-input converter families are derived by hybridizing two conventional converters. However, the filter capacitor is linked with two different converters and becomes the challenging task to maintain a constant voltage across the filter capacitor. Moreover, some configurations also required a large number of reactive, and semiconductor components along with the transformer, i.e. decrease the efficiency and make circuit again bulky. In [17], multi-port converter configurations are proposed by the hybridization of the full-bridge and bi-directional DC-DC converter. The complex power circuitry and control are the main drawback of these converters. In addition, a large number of reactive components and semiconductor devices, along with an isolated transformer, are required. Hence, the circuitry is bulky with increased losses.

In [18], dual output single input three-level DC-DC converter proposed. It is a hybrid combination of three-level buck and boost converters. The voltage stress of switches is reduced, but the sophisticated control and voltage balancing of the output side capacitor is the challenging task for this converter. Moreover, the converter failed to function if anyone device fails. In [19], the decoupled tri-port converter is proposed by using two buck-boost converters and an isolated full-bridge converter. The number of power switches is reduced, and soft switching is achieved. However, the selection of isolated transformer, power-sharing between two converters, and sophisticated control are difficult tasks.

In [20], the isolated converter is proposed with high efficiency using a boost-flyback configuration. However, the configuration required an isolated transformer, which undoubtedly increases the size and cost of the converter and makes the system bulky. Moreover, the saturation of transformer and leakage reactance will limit the performance of the converter. Therefore, the selection of isolated transformer and sophisticated control is a difficult task. Recently, various DC-DC converters also proposed in [21]–[25] with a high voltage conversion ratio. On applications, with variation in the irradiations, it becomes necessary to extract maximum power from the PV panel by tracking Maximum Power Point (MPP) using tracking algorithms. Incremental-conductance, hill climbing, and Perturb & Observe (P&O) algorithms are well-liked Maximum Power Point Tracking (MPPT) algorithms by their simplicity and easy implementation. Based on the power increase/decrease perturbation condition, the MPPT controller generates pulses for the DC-DC converter to locate MPP. Accordingly, the power and voltage slope used to decide the next perturbation should be and to locate MPP. Fig. 1(c) depicts the concept to track MPP by using P-V and I-V characteristics of the PV panel.

In light of the advantages of the tri-port DC-DC converter, this paper presents a new triple-port converter. The proposed configuration is derived by integrating buck-boost converter with a bi-directional boost converter for harnessing and storage of PV energy. It also aims at storing the energy and further used during energy deficiency. The advantage of the proposed converter holds the higher conversion gain, simple working, and mode of control are adjusted by switching for the power

TABLE 1. Summary of modes of operation of proposed triple port converter.

Modes	Input Port	Output Port	Power flow direction	Type of Mode
Mode-1	Port -1	Port-3	PV panel to Load	Single Input Single Output (SISO-1)
Mode-2	Port -2	Port-3	Battery to Load	Single Input Single Output (SISO-2)
Mode-3	Port -1	Port -2 and Port -3	PV panel to Load and Battery	Single Input Dual Output (SIDO)
Mode-4	Port -1 and Port -2	Port-3	PV panel and Battery to Load	Dual Input Single Output (DISO)

flow direction. Furthermore, the proposed triple port converter is designed by using conventional power converters, i.e. simple circuitry arrangement, and the principles used in [9], [16] and [26] are integrated to form the basis collectively. The buck-boost structure is chosen because of the suitability for the applications with overlapping source and load voltages.

II. PROPOSED TRIPLE PORT DC-DC BUCK-BOOST CONVERTER

Fig. 1(d) shows the power circuit of the proposed triple port DC-DC converter. It consists of four power-controlled switches (S_1, S_2, S_c, and S_d), three inductors (L_1, L_2, and L_3), two capacitors (C_1 and C_0), four uncontrolled switches (D_1, D_2, Dc and D_d, including antiparallel diode of MOSFET's) and a resistive load R. The power switches S_1 and S_2 are controlled synchronously to transfer the power from Port-1 to other ports. The proposed converter has two unidirectional (Port-1 and 3) and one bi-directional port (Port-2); where Port-1 is, input Port and Port-3 is output port. Thus, photovoltaic panel and load are connected at the Port-1 and Port-3, respectively, and the battery is connected at Port-2. Thus, when the energy in the battery is less, the PV panel provides energy to load. It is assumed that the converter is operating in steady-state, all the capacitors are large enough to keep the voltage across them with fewer ripples, and all the components are ideal. In the power circuit, the connection of S_1, L_1, D_1 and C_1 forms the conventional unidirectional buck-boost converter and the connection of L_3, S_d and S_c form the bi-directional boost converter. Additionally, L_2, S_2, and D_2 are connected to enhance the power flow and voltage conversion capability of the buck-boost converter. Consider the case, when the PV power is just sufficient only to supply the load demand, and the battery has less charge. During this situation, all PV power must be directed to load, and the battery should be completely isolated; otherwise, reverse current flow through the body diode of switch S_c. Notably, battery isolation and battery charging/discharging operation can be possible in a simple mode: turn off both S_d, and S_c switches. In this case, no energy transfer will be made either from or to the battery. The only condition for battery isolation with S_c and S_d off is that battery voltage to be lower than the voltage on Co. As per Table 1, this condition is always met as V_{Bt} is lesser than V_{CO}. Also, turning off the switches S_c and S_d prevent the battery from overcharging and deep discharging.

III. ANALYSIS OF PROPOSED TRIPLE PORT DC-DC CONVERTER

The different modes of operation with their switching states and equivalent circuit diagrams are explained in this section. In Table 1, modes of operation of the proposed DC-DC converter are provided with information of ports and power flow direction in the converter.

A. MODE-1 (PV TO LOAD)

In mode-1, the PV panel (Port-1) delivers power to the load (Port-3). The power flow from the PV panel to load is maintained by controlling switches S_1, and S_2 are simultaneously turned ON and OFF. Thus, this mode is divided into two states; one when both switches are turned ON (duty cycle for state-1 is k_1) and another when they are turned OFF (duty cycle for state-2 is k_2), hence, $k_1 + k_2 = 1$. The battery disconnected in this mode and switches S_C and S_d are in OFF state. The equivalent circuit when switches S_1, S_2 simultaneously are turned ON and OFF is shown in Fig. 2(a) and 2(b) respectively. The characteristics waveforms of mode-1 are shown in Fig. 2(c). When switches S_1 and S_2 are turned ON, inductor L_1 is magnetized by input supply (V_{PV}) and inductor L_2 is magnetized by input supply (V_{PV}) and capacitor C_1 voltage. Diode D_1, D_2, D_c, and D_d are in reverse biased. The inductor (L_1 and L_2) current slope and capacitor (C_0 and C_1) voltage slope in ON state obtained as,

$$\left.\begin{aligned} \frac{di_{L1}}{dt} &= \frac{V_{PV}}{L_1}, \ \frac{dv_{C0}}{dt} = \frac{-V_o}{RC_0} \\ \frac{di_{L2}}{dt} &= \frac{V_{PV}+V_{C1}}{L_2}, \ \frac{dv_{C1}}{dt} = \frac{-i_{L2}}{C_1} \end{aligned}\right\} \tag{1}$$

When switches S_1 and S_2 are turned OFF, inductor L_1 is demagnetized to charge capacitor C_1. Inductor L_2 is demagnetized through the load and also charging the capacitor C_0. Diodes D_1, D_2 are forward biased, and diodes D_c, and D_d are reversed biased. The inductors (L_1 and L_2) current slope and capacitors ($C_0$and C_1) voltage slope in OFF state are obtained as,

$$\left.\begin{aligned} \frac{di_{L1}}{dt} &= \frac{-V_{C1}}{L_1}, \ \frac{dv_{C0}}{dt} = \frac{i_{L2}-V_0R^{-1}}{C_0} \\ \frac{di_{L2}}{dt} &= \frac{-V_0-V_{C1}}{L_2}, \ \frac{dv_{C1}}{dt} = \frac{i_{L1}+i_{L2}}{C_1} \end{aligned}\right\} \tag{2}$$

The voltage across the capacitors (C_0 and C_1) is obtained as,

$$V_{C1} = \frac{k_1}{1-k_1}V_{PV}, \quad V_{C0} = \left(\frac{k_1}{1-k_1}\right)^2 V_{PV} \tag{3}$$

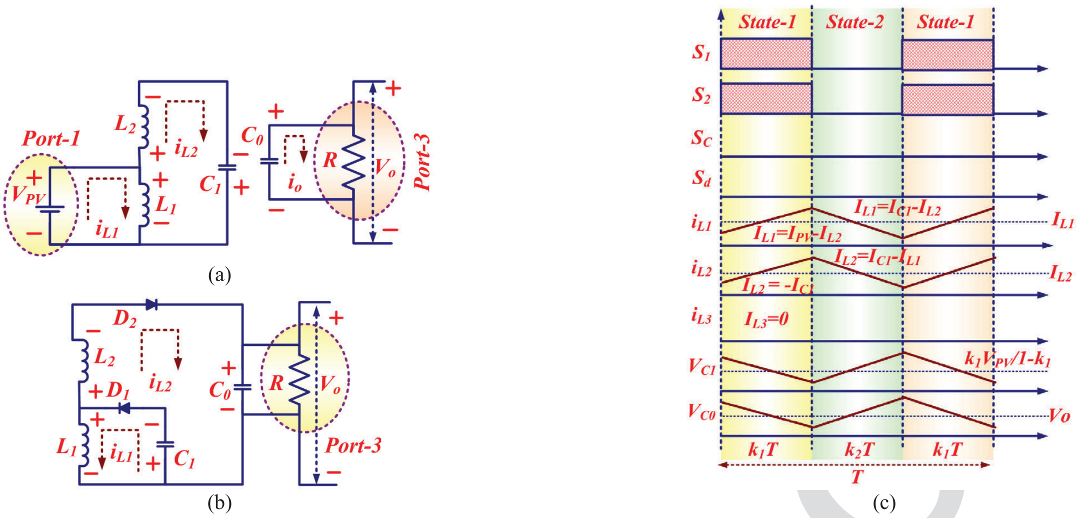

FIGURE 2. Mode-1 equivalent circuit of the proposed converter (a) When Switches S_1 and S_2 are ON (State-1), (b) When switches S_1 and S_2 are in OFF (State-2), (c) Characteristic waveforms for mode-1.

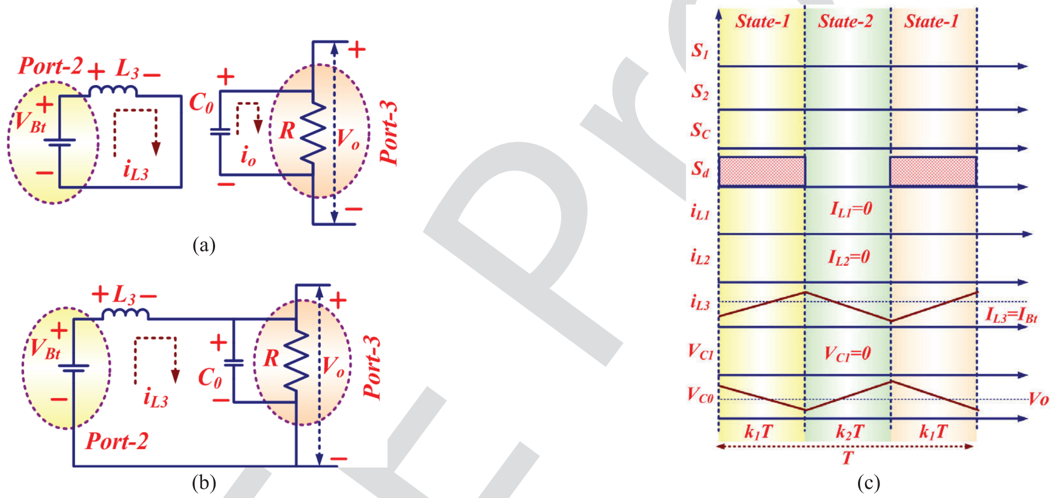

FIGURE 3. Mode-2 equivalent circuit of the proposed converter (a) When switch S_d is ON (State-1), (b) When switch S_d is OFF (State-2), (c) Characteristic waveform for mode-2.

The drain to source voltage across switches and Peak Inverse Voltage (PIV) of diodes is obtained as,

$$\left.\begin{array}{l} V_{S1} = V_{C1} + V_{PV}, V_{S2} = V_{C1} + V_0, \\ -V_{Si} = V_{Sc} = V_{Sd} = V_0/3 \\ V_{D1} = -\left(V_{C1} + V_{PV}\right), V_{D2} = -\left(V_{C1} + V_0\right) \end{array}\right\} \quad (4)$$

B. MODE-2 (BATTERY TO LOAD)

In mode-2, the battery (Port-2) delivers power to the load (Port-3). This happens during the absence of sufficient PV power. The power flow of battery to load is maintained by controlling switch S_d. This mode is divided into two states; one when switch S_d is turned ON (duty cycle for state-1 is k_1) and another when switch S_d is OFF (duty cycle for state-2 is k_2), hence, $k_1 + k_2 = 1$. Switch S_d is turned ON; diode D_c plays a critical role to connect inductor L_3 to load.

The equivalent circuit when switch S_d is turned ON is shown in Fig. 3(a). In this case, inductor L_3 is magnetized by battery supply (V_{Bt}), and capacitor C_0 is discharged through the load. Diodes D_1, D_2,D_c, and D_d are reversed biased. The inductor (L_3) current slope and capacitor (C_0) voltage slope is obtained as,

$$\frac{di_{L3}}{dt} = \frac{V_{Bt}}{L_3}, \quad \frac{dv_{C0}}{dt} = \frac{-V_o}{RC_0} \quad (5)$$

The equivalent circuit when switch S_d turned OFF is shown in Fig. 3(b). In this case, inductor L_3 is demagnetized in series with battery (V_{Bt}) and transfers its energy to charge capacitor C_0 through diode D_c. Diode D_1, D_2, and D_d are reverse biased. The inductor (L_3) current slope and capacitor (C_0) voltage slope are obtained as,

$$\frac{di_{L3}}{dt} = \frac{-V_o + V_{Bt}}{L_3}, \quad \frac{dv_{C0}}{dt} = \frac{i_{L3} - V_oR^{-1}}{C_0} \quad (6)$$

The voltage across the capacitor (C_0) is obtained as,

$$V_{C0} = \frac{1}{1-k_1}V_{Bt} \quad (7)$$

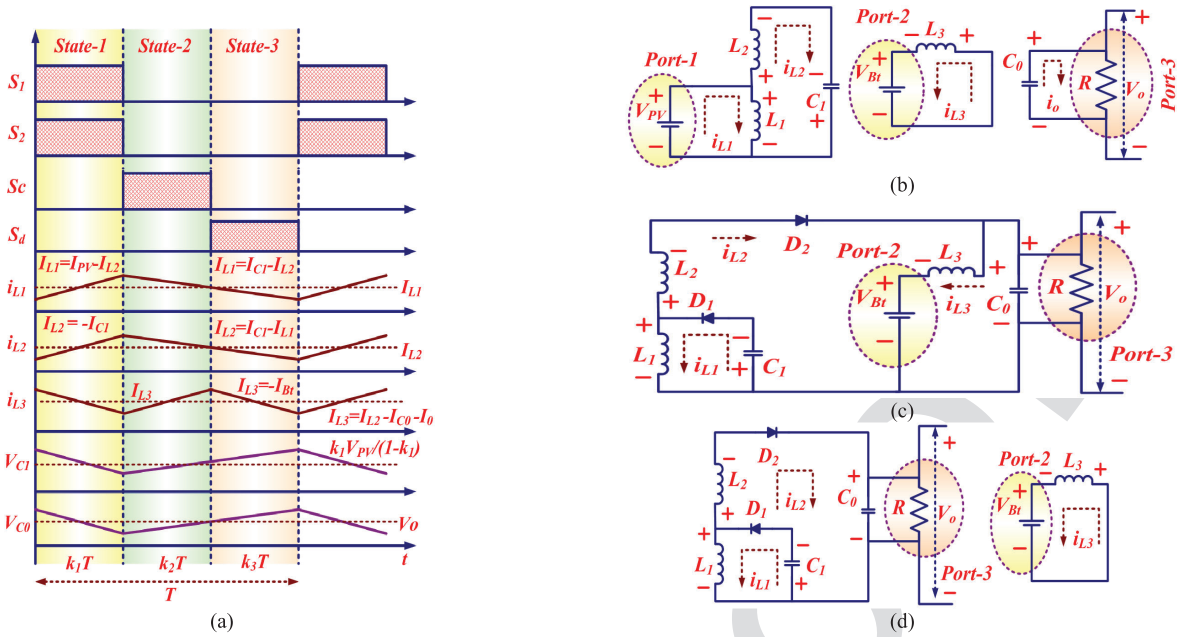

FIGURE 4. Mode-3 equivalent circuit of proposed converter (a) Characteristic waveform for mode-3 (b) State-1 (c) State-2 (d) State-3.

The drain to source voltage across switches and PIV of diodes are obtained as,

$$V_{Sd} = V_0, \quad V_{Si} = V_{Sc} = V_0/2 \tag{8}$$

The characteristics waveforms of mode-2 are shown in Fig. 3(c).

C. MODE-3 (PV TO BATTERY AND LOAD)

Depending on the switching states, this mode consists of three sub-states (duty cycles for state-1, state-2, and state-3 are k_1, k_2, and k_3 respectively; hence, $k_1 + k_2 + k_3 = 1$) and characteristics waveforms for mode-3 are shown in Fig. 4(a). At the Port-1 and Port-3 photovoltaic panel and load are connected, respectively, and the battery is connected at Port-2.

1) STATE-1

In this state, switches S_1 and S_2 are synchronously turned ON. Diodes D_1, D_2 and D_c are reversed biased, and diode D_d is in forward biased condition. Inductor L_1 is magnetized by input supply (V_{PV}) through switch S_1. Inductor L_2 is magnetized by input supply (V_{PV}) and capacitor C_1 through switch S_2. Thus, the slope of the inductor L_1 and L_2 current is positive. Capacitor C_0 is discharged to make the load voltage constant. The power switches S_c, and S_d are turned OFF.

The inductor L_3 is demagnetized through diode D_d and supply power to charge the battery (Port-2). Thus, the slope of the inductor L_3current is negative, and diode D_d is forward biased. The equivalent circuit diagram for this state is shown in Fig. 4(b). The inductor (L_1, L_2, and L_3) current slopes and capacitor (C_0 and C_1) voltage slopes for this state are obtained as,

$$\left.\begin{array}{l} \dfrac{di_{L1}}{dt} = \dfrac{V_{PV}}{L_1}, \dfrac{di_{L2}}{dt} = \dfrac{V_{PV}+V_{C1}}{L_2}; \dfrac{di_{L3}}{dt} = \dfrac{-V_{Bt}}{L_3} \\ \dfrac{dv_{C0}}{dt} = \dfrac{-V_o}{RC_0}, \dfrac{dv_{C1}}{dt} = \dfrac{-i_{L2}}{C_1} \end{array}\right\} \tag{9}$$

2) STATE-2

The power switches S_1 and S_2 are synchronously turned OFF. Diodes D_1 and D_2 are forward biased and diodes D_c, D_d is reversed biased. Inductor L_1 is demagnetized to charge the capacitor C_1 through diode D_1. Inductor L_2 is demagnetized to charge the capacitors C_0 through diode D_2. Switch S_c is turned ON and switch S_d is turned OFF. Inductor L_3 is magnetized, and the battery is charged by inductor L_2 through switch S_c. As a result, the slope of inductor (L_1 and L_2) current is negative, and the slope of inductor L_3 is positive. The equivalent circuit diagram for this state is shown in Fig. 4(c). The inductor (L_1, L_2, and L_3) current slope and capacitor (C_0 and C_1) voltage slope for this state is obtained as,

$$\left.\begin{array}{l} \dfrac{di_{L1}}{dt} = \dfrac{-V_{C1}}{L_1}, \dfrac{di_{L2}}{dt} = \dfrac{-V_0-V_{C1}}{L_2}, \dfrac{di_{L3}}{dt} = \dfrac{V_0-V_{Bt}}{L_3} \\ \dfrac{dv_{C0}}{dt} = \dfrac{i_{L2}-i_{L3}-V_0R^{-1}}{C_0}, \dfrac{dv_{C1}}{dt} = \dfrac{i_{L1}+i_{L2}}{C_1} \end{array}\right\} \tag{10}$$

3) STATE-3

In this state, switches S_1, S_2, S_d, and S_c are turned OFF. In this state, inductors L_1 and L_2 are demagnetized to charge capacitors C_1 and C_0 respectively. The inductor L_3 is demagnetized, and energy is transferred to charge the battery through diode D_d. Thus, the slopes of the inductors L_1, L_2 and L_3 currents are negative. Diodes D_1, D_2, and D_d are forward biased, and diodes D_C are reversed biased. The equivalent circuit diagram

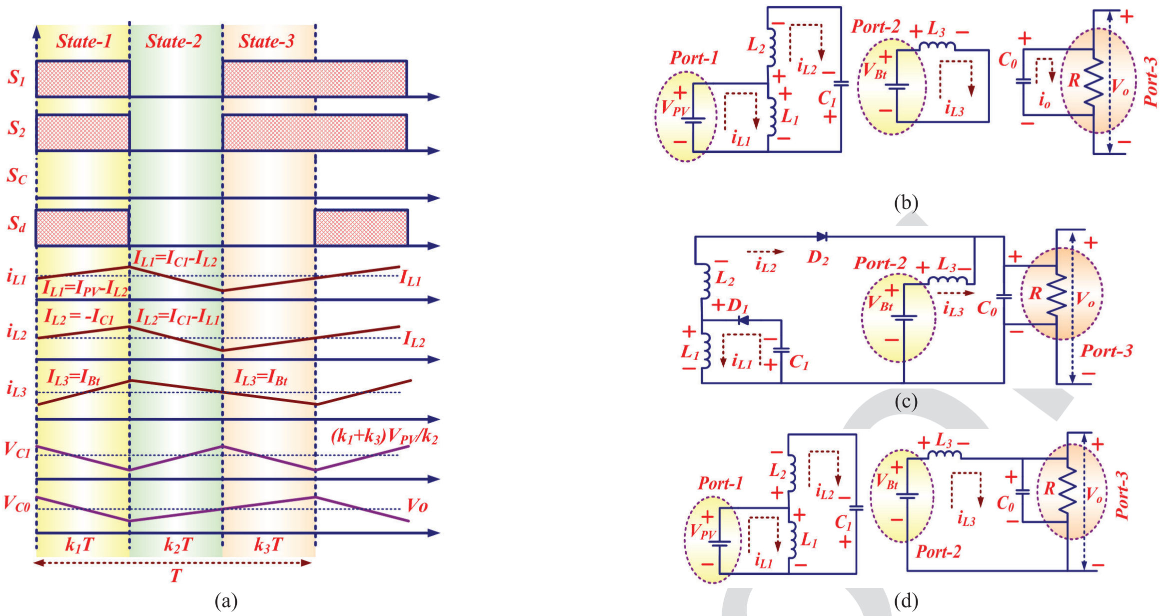

FIGURE 5. Mode-4 equivalent circuit of proposed converter (a) Characteristic waveform for mode-4 (b) State-1 (c) State-2 (d) State-3.

for this state is shown in Fig. 4(d). The inductor (L_1, L_2, and L_3) current slope and capacitor (C_0 and C_1) voltage slope for this state is obtained as,

$$\left.\begin{aligned} &\frac{di_{L1}}{dt}=\frac{-V_{C1}}{L_1},\ \frac{di_{L2}}{dt}=\frac{-V_0-V_{C1}}{L_2},\ \frac{di_{L3}}{dt}=\frac{-V_{Bt}}{L_3}\\ &\frac{dv_{C0}}{dt}=\frac{i_{L2}-V_0R^{-1}}{C_0},\ \frac{dv_{C1}}{dt}=\frac{i_{L1}+i_{L2}}{C_1}\end{aligned}\right\} \quad (11)$$

The voltage across capacitors (C_0 and C_1) and battery voltage (V_{Bt}) are obtained as,

$$\left.\begin{aligned} &V_{C1}=\frac{k_1}{1-k_1}V_{PV},\ V_{C0}=\left(\frac{k_1}{1-k_1}\right)^2 V_{PV}\\ &V_{Bt}=(k_2)\left(\frac{k_1}{1-k_1}\right)^2 V_{PV}\end{aligned}\right\} \quad (12)$$

The drain to source voltage magnitude across switches and PIV of diodes are obtained as

$$\left.\begin{aligned} &V_{S1}=V_{C1}+V_{PV},\ V_{S2}=V_{C1}+V_0,\ -V_{Si}=V_{Sc}=V_0/2,\\ &V_{Sd}=V_0,\ V_{D1}=-\left(V_{C1}+V_{PV}\right),\ V_{D2}=-\left(V_{C2}+V_0\right)\end{aligned}\right\} \quad (13)$$

D. MODE-4 (PV AND BATTERY TO LOAD)

This mode is employed when the PV energy is not sufficient to drive the load. Also, Port-1 and Port-2 are the input ports, and Port-3 is the output port. Depending on the switching states, this mode is divided into three sub-states (duty cycles for state-1, state-2, and state-3 are k_1, k_2, and k_3 respectively; hence, $k_1 + k_2 + k_3 = 1$) and characteristics waveforms of the converter are shown in Fig. 5(a).

1) STATE-1

In this state, switches S_1, S_2, and S_d are turned ON. Inductor L_1 is magnetized by input supply (V_{PV}) through switch S_1. At the same time, inductor L_2 is magnetized by input supply (V_{PV}) and capacitors C_1 through switch S_2. Capacitor C_0 is discharged through load R. The inductor L_3 is magnetized by battery voltage (V_{Bt}) through switch S_d. Therefore, in this state slope of the inductors L_1, L_2 and L_3 current is positive. In this state, switch S_c is turned OFF, and diodes D_1, D_2, D_c, and D_d are reversed biased. The equivalent circuit diagram for this state is shown in Fig. 5(b). The inductor (L_1, L_2, and L_3) current slope and capacitor ($C_0$and C_1) voltage slope for this state is obtained as,

$$\left.\begin{aligned} &\frac{di_{L1}}{dt}=\frac{V_{PV}}{L_1},\ \frac{di_{L2}}{dt}=\frac{V_{PV}+V_{C1}}{L_2},\ \frac{di_{L3}}{dt}=\frac{V_{Bt}}{L_3}\\ &\frac{dv_{C0}}{dt}=\frac{-V_o}{RC_0},\ \frac{dv_{C1}}{dt}=\frac{-i_{L2}}{C_1}\end{aligned}\right\} \quad (14)$$

2) STATE-2

In this state, switches S_1 and S_2 are synchronously turned OFF. Inductors L_1 and L_2 are demagnetized to charge the capacitors C_1 and C_0, respectively. Switches S_C *and* S_d are turned OFF. Inductor L_3 is also demagnetized to supply load. Therefore, in this state slope of the inductor L_1, L_2 and L_3 currents are negative. In this state, the circuit from the battery (Port-2) to load (Port-3) is acting as a conventional boost converter; diodes D_1, D_2, D_C are forward biased, and diode D_d is reverse biased. As a result, the load is supplied throughout the state by battery and inductor L_2. The equivalent circuit diagram for this state is shown in Fig. 5(c). The inductors (L_1, L_2, and L_3) current slope and capacitors (C_0 and C_1) voltage slope for this state is obtained as,

$$\left.\begin{aligned} &\frac{di_{L1}}{dt}=\frac{-V_{C1}}{L_1},\ \frac{di_{L2}}{dt}=\frac{-V_0-V_{C1}}{L_2},\ \frac{di_{L3}}{dt}=\frac{V_{Bt}-V_0}{L_3}\\ &\frac{dv_{C0}}{dt}=\frac{i_{L2}+i_{L3}-V_0R^{-1}}{C_0},\ \frac{dv_{C1}}{dt}=\frac{i_{L1}+i_{L2}}{C_1}\end{aligned}\right\} \quad (15)$$

3) STATE-3

In this state, switches S_1 and S_2 are synchronously turned ON. Inductor L_1 is magnetized by input supply (V_{PV}) through switch S_1. Inductor L_2 is magnetized by input supply (V_{PV}) and capacitors C_1 through switch S_2. Switches S_C and S_d are turned OFF. Inductor L_3 is demagnetized to supply load. Therefore, the slope of the inductor L_1, L_2 current is positive, and inductor L_3 current is negative. The circuit from the battery (Port-2) to load (Port-3) is acting as a conventional boost converter. In this state, diode D_c is forward biased, and diodes D_1, D_2, and D_d are reversed biased. Thus, the load is supplied by battery throughout the state. The equivalent circuit diagram for this state is shown in Fig. 5(d). The inductors (L_1, L_2, and L_3) current slope and capacitors (C_0 and C_1) voltage slope for this state is obtained as,

$$\left.\begin{array}{l}\dfrac{di_{L1}}{dt}=\dfrac{V_{PV}}{L_1},\ \dfrac{di_{L2}}{dt}=\dfrac{V_{PV}+V_{C1}}{L_2},\ \dfrac{di_{L3}}{dt}=\dfrac{V_{Bt}-V_o}{L_3}\\ \dfrac{dv_{C0}}{dt}=\dfrac{i_{L3}-V_0R^{-1}}{C_0},\ \dfrac{dv_{C1}}{dt}=\dfrac{-i_{L2}}{C_1}\end{array}\right\} \quad (16)$$

The voltage across the capacitors (C_1 and C_0) is obtained as,

$$\left.\begin{array}{l}V_{C1}=\dfrac{k_1+k_3}{1-(k_1+k_3)}V_{PV}\\ V_{C0}=\left(\dfrac{k_1+k_3}{1-(k_1+k_3)}\right)^2V_{PV}=\dfrac{1}{1-k_1}V_{Bt}\end{array}\right\} \quad (17)$$

The drain to source voltage magnitude across switches and PIV of diodes are obtained as,

$$\left.\begin{array}{l}V_{S1}=V_{C1}+V_{PV}\\ V_{S2}=V_{C1}+V_0,-V_{Si}=V_{Sc}=V_0/2,\ V_{Sd}=V_0\\ V_{D1}=-\left(V_{C1}+V_{PV}\right),\ V_{D2}=-\left(V_{C1}+V_0\right)\end{array}\right\} \quad (18)$$

E. DESIGN OF INDUCTORS

In general, k_{Sx} is the duty cycle of switch S_x and thus $k_{Sx}+k'_{Sx}=1$. The inductors are designed to ensure the condition that the peak-to-peak inductor current variation, $\Delta i_{L(peak-peak)}$ is within 20% of the average inductor current. The critical point between positive current and negative current in the inductor is assumed at $\Delta i_L = 10\%$ of the rated dc current. In addition, the maximum possible input voltage has been used for calculations. The desired current ripple of inductor and inductor volt-sec balance principle is used to design inductor L_1 as:

$$\Delta i_{L1}=\frac{V_{PV}}{L_1}k_{S1}T=\frac{V_{PV}}{L_1f_s}k_{S1}\Rightarrow L_1=\frac{V_{PV}}{\Delta i_{L1}\times f_s}k_{S1} \quad (19)$$

where Δi_{L1} is a ripple of inductor L_1 current. Similarly, the current ripple inductor L_2 and its slope are used to design inductor L_2 as

$$\left.\begin{array}{l}\Delta i_{L2}=\dfrac{V_{PV}+V_{C1}}{L_2}k_{S2}T=\dfrac{\left(1+\dfrac{k_{S1}}{1-k_{S1}}\right)V_{PV}}{L_2f_s}k_{S2}\\ L_2=\dfrac{V_{PV}+V_{C1}}{\Delta i_{L2}\times f_s}k_{S2},\ V_{C1}=\dfrac{k_{S1}}{1-k_{S1}}V_{PV}\end{array}\right\} \quad (20)$$

where Δi_{L2} is a ripple of inductor L_2 current. Similarly, Volt-sec balance and desired current ripple on inductor L_3 are used to design L_3 as

$$\Delta i_{L3}=\frac{V_{Bt}}{L_3}k_{Sd}T=\frac{V_{Bt}}{L_3\times f_s}k_{Sd}\Rightarrow L_3=\frac{V_{Bt}}{\Delta i_{L3}\times f_s}k_{Sd} \quad (21)$$

where Δi_{L3} is a ripple of inductor L_3 current.

F. DESIGN OF CAPACITORS

The capacitor charge-sec balance and the voltage ripples of capacitor C_1 are used to design capacitor C_1 as,

$$\left.\begin{array}{l}\Delta V_{C1}=\dfrac{i_{L2}}{C_1}k_{S1}T=\dfrac{V_0}{RC_1f_s(1-k_{S1})}k_{S1}\\ C_1=\dfrac{V_0}{R\Delta V_{C1}f_s(1-k_{S1})}k_{S1}\end{array}\right\} \quad (22)$$

The voltage ripples of capacitor C_0 and its slope are used to design capacitor C_0 as,

$$\Delta V_{C0}=\frac{V_0}{RC_0}k_{S2}T=\frac{V_0}{RC_0f_s}k_{S2},\quad C_0=\frac{V_0}{R\Delta V_{C0}f_s}k_{S2} \quad (23)$$

The voltage and current stress across switches are diodes is calculated as follows,

$$V_{S1}=V_{D1}=\frac{1}{1-d_1}V_{PV},\ V_{S2}=V_{D2}=\frac{1}{d_1}V_o \quad (24)$$

$$I_{S1}=\frac{d_1^4}{(1-d_1)^4}\frac{V_{PV}}{R},\ I_{S2}=I_{D1}=\frac{d_1^3}{(1-d_1)^3}\frac{V_{PV}}{R},$$

$$I_{D2}=\frac{d_1^2}{(1-d_1)^2}\frac{V_{PV}}{R} \quad (25)$$

IV. STATE SPACE ANALYSIS OF PROPOSED THREE PORT DC-DC CONVERTER

In [27], by using the state-space averaging method, a hybrid PV/wind battery charger is presented with a mathematical background. In this section, the state space analysis of the proposed triple port converter is discussed for each mode. Let us consider $x(t)$ is state vector and $u(t)$ is input vector. The state variables are inductor currents and capacitor voltages. In general, when the switch is ON and OFF, the circuit is illustrated by the state space equation as follows,

$$\left.\begin{array}{l}ON\ state\left\{\begin{array}{l}K\dot{x}(t)=A'x(t)+B'u(t)\\ y(t)=C'x(t)+D'u(t)\end{array}\right.\\ OFF\ state\left\{\begin{array}{l}K\dot{x}(t)=A"x(t)+B"u(t)\\ y(t)=C"x(t)+D"u(t)\end{array}\right.\end{array}\right\} \quad (26)$$

A. MODE-1 (PV TO LOAD)

In this mode, the converter is operated as SISO converter; where PV is, the input port and load is the output port. When switches S_1 and S_2 are simultaneously turned ON, the state-space matrices are obtained as (27), shown at the bottom of the next page. When switches S_1 and S_2 are simultaneously turned OFF, the state-space matrices are obtained as (28), shown at the bottom of the next page. By (27)-(28), the voltage and current conversion ratio are obtained as (29).

$$\frac{V_{C1}}{V_{PV}}=\frac{k_1}{1-k_1},\quad \frac{V_{C0}}{V_{PV}}=\left(\frac{k_1}{1-k_1}\right)^2,\ \frac{I_0}{I_{PV}}=\left(\frac{1-k_1}{k_1}\right)^2 \quad (29)$$

B. MODE-2 (BATTERY TO LOAD)

In this mode, the converter is operated as SISO converter; where the battery is an input port and load is output port. When switch S_d is turned ON, the state-space matrices are obtained as follow,

$$\begin{bmatrix} \dot{i}_{L3}(t) \\ \dot{v}_{C0}(t) \end{bmatrix} = \underbrace{\begin{bmatrix} 0 & 0 \\ 0 & \frac{-1}{RC_0} \end{bmatrix}}_{A'} \begin{bmatrix} i_{L3}(t) \\ v_{C0}(t) \end{bmatrix} + \underbrace{\begin{bmatrix} \frac{1}{L_3} \\ 0 \end{bmatrix}}_{B'} [V_{Bt}] \quad (30)$$

$$\begin{bmatrix} i_{Bt} \\ Vo \end{bmatrix} = \underbrace{\begin{bmatrix} 1 & 0 \\ 0 & 1 \end{bmatrix}}_{C'} \begin{bmatrix} i_{L3}(t) \\ v_{C0}(t) \end{bmatrix} + \underbrace{\begin{bmatrix} 0 \\ 0 \end{bmatrix}}_{D'} [V_{Bt}] \quad (31)$$

When switch S_d is turned OFF, the state-space matrices are obtained as follows,

$$\begin{bmatrix} \dot{i}_{L3}(t) \\ \dot{v}_{C0}(t) \end{bmatrix} = \underbrace{\begin{bmatrix} 0 & \frac{-1}{L_3} \\ \frac{1}{C_0} & \frac{-1}{RC_0} \end{bmatrix}}_{A''} \begin{bmatrix} i_{L3}(t) \\ v_{C0}(t) \end{bmatrix} + \underbrace{\begin{bmatrix} \frac{1}{L_3} \\ 0 \end{bmatrix}}_{B''} [V_{Bt}] \quad (32)$$

$$\begin{bmatrix} i_{Bt} \\ Vo \end{bmatrix} = \underbrace{\begin{bmatrix} 1 & 0 \\ 0 & 1 \end{bmatrix}}_{C''} \begin{bmatrix} i_{L3}(t) \\ v_{C0}(t) \end{bmatrix} + \underbrace{\begin{bmatrix} 0 \\ 0 \end{bmatrix}}_{D''} [V_{Bt}] \quad (33)$$

By (30)-(33), the voltage and current conversion ratio are obtained as,

$$\frac{V_{C0}}{V_{Bt}} = \frac{1}{1-k_1}, \quad \frac{I_0}{I_{Bt}} = 1-k_1 \quad (34)$$

C. MODE-3 (PV TO BATTERY AND LOAD)

In this mode, the converter is operated as SIDO converter; where PV is input port, battery and load are output ports. When switches S_1, S_2, and S_d are simultaneously turned ON, the state-space matrices are obtained as (35), shown at the bottom of the next page. When switches S_1, S_2, and S_d are simultaneously turned OFF, the state-space matrices are obtained as (36), shown at the bottom of the next page. When switches S_1, S_2 are turned OFF, and S_d is ON the state-space matrices are obtained as (37), shown at the bottom of the page 11.

Using (35)-(37), the voltage and current conversion ratio are obtained as,

$$\frac{V_{Bt}}{V_{PV}} = \left(\frac{\sqrt{k_2}k_1}{1-k_1}\right)^2, \quad \frac{V_{C0}}{V_{PV}} = \frac{I_{PV}}{I_0} = \left(\frac{k_1}{1-k_1}\right)^2 \quad (38)$$

D. MODE-4 (PV AND BATTERY TO LOAD)

In this mode, the converter is operated as DISO converter; where PV and battery are input ports and load is an

$$\begin{bmatrix} \dot{i}_{L1}(t) \\ \dot{i}_{L2}(t) \\ \dot{i}_{L3}(t) \\ \dot{v}_{C1}(t) \\ \dot{v}_{C0}(t) \end{bmatrix} = \underbrace{\begin{bmatrix} 0 & 0 & 0 & 0 & 0 \\ 0 & 0 & 0 & \frac{1}{L_2} & 0 \\ 0 & 0 & 0 & 0 & 0 \\ 0 & \frac{-1}{C_1} & 0 & 0 & 0 \\ 0 & 0 & 0 & 0 & \frac{-1}{R_L C_0} \end{bmatrix}}_{A'} \begin{bmatrix} i_{L1}(t) \\ i_{L2}(t) \\ i_{L3}(t) \\ v_{C1}(t) \\ v_{C0}(t) \end{bmatrix} + \underbrace{\begin{bmatrix} \frac{1}{L_1} \\ \frac{1}{L_2} \\ 0 \\ 0 \\ 0 \end{bmatrix}}_{B'} [V_{PV}],$$

$$\begin{bmatrix} i_{PV} \\ Vo \end{bmatrix} = \underbrace{\begin{bmatrix} 1 & 1 & 0 & 0 & 0 \\ 0 & 0 & 0 & 0 & 1 \end{bmatrix}}_{C'} \begin{bmatrix} i_{L1}(t) \\ i_{L2}(t) \\ i_{L3}(t) \\ v_{C1}(t) \\ v_{C0}(t) \end{bmatrix} + \underbrace{\begin{bmatrix} 0 \\ 0 \end{bmatrix}}_{D'} [V_{PV}] \quad (27)$$

$$\begin{bmatrix} \dot{i}_{L1}(t) \\ \dot{i}_{L2}(t) \\ \dot{i}_{L3}(t) \\ \dot{v}_{C1}(t) \\ \dot{v}_{C0}(t) \end{bmatrix} = \underbrace{\begin{bmatrix} 0 & 0 & 0 & \frac{-1}{L_1} & 0 \\ 0 & 0 & 0 & \frac{-1}{L_2} & \frac{-1}{L_2} \\ 0 & 0 & 0 & 0 & 0 \\ \frac{1}{C_1} & \frac{1}{C_1} & 0 & 0 & 0 \\ 0 & \frac{1}{C_0} & 0 & 0 & \frac{-1}{R_L C_0} \end{bmatrix}}_{A"} \begin{bmatrix} i_{L1}(t) \\ i_{L2}(t) \\ i_{L3}(t) \\ v_{C1}(t) \\ v_{C0}(t) \end{bmatrix} + \underbrace{\begin{bmatrix} 0 \\ 0 \\ 0 \\ 0 \\ 0 \\ 0 \end{bmatrix}}_{B"} [V_{PV}],$$

$$\begin{bmatrix} i_{PV} \\ Vo \end{bmatrix} = \underbrace{\begin{bmatrix} 0 & 0 & 0 & 0 & 0 \\ 0 & 0 & 0 & 0 & 1 \end{bmatrix}}_{C"} \begin{bmatrix} i_{L1}(t) \\ i_{L2}(t) \\ i_{L3}(t) \\ v_{C1}(t) \\ v_{C0}(t) \end{bmatrix} + \underbrace{\begin{bmatrix} 0 \\ 0 \end{bmatrix}}_{D"} [V_{PV}] \quad (28)$$

output port. Both input ports share the output current. When switches S_1, S_2, and S_d are simultaneously turned ON, the state-space matrices are obtained as (39), shown at the bottom of the page 11. When switches S_1, S_2, and S_d are simultaneously turned OFF, the state-space matrices are obtained as (40), shown at the bottom of the page 11. When Switches S_1, S_2 are turned ON, and S_d is OFF the state-space matrices are obtained as (41), shown at the bottom of the page 12. The voltage conversion ratio is obtained as,

$$\frac{V_{C0}}{V_{Bt}} = \frac{1}{1-k_1}, \quad \frac{V_{C0}}{V_{PV}} = \frac{I_{PV}}{I_0} = \left(\frac{(k_1+k_3)}{1-(k_1+k_3)}\right)^2 \tag{42}$$

V. HARDWARE IMPLEMENTATION AND EXPERIMENTAL RESULTS

The system-level control block diagram for the proposed TPC and control logic algorithm for mode selection is given in Fig. 6(a)-(b) respectively. The multi-objective control algorithm was designed to achieve the battery management, the direction of power flow, mode of operation and duty cycle selection. The selection of the mode of operation and the corresponding switching signals are made based on the present PV power, SOC or maximum current pre-set of battery and the load demand. A simple voltage control method is used to maintain output voltage, in which an error signal is generated by the comparing output voltage against a reference voltage.

$$\begin{bmatrix} \dot{i}_{L1}(t) \\ \dot{i}_{L2}(t) \\ \dot{i}_{L3}(t) \\ \dot{v}_{C1}(t) \\ \dot{v}_{C0}(t) \\ \dot{v}_{CBt}(t) \end{bmatrix} = \underbrace{\begin{bmatrix} 0 & 0 & 0 & 0 & 0 & 0 \\ 0 & 0 & 0 & \frac{1}{L_2} & 0 & 0 \\ 0 & 0 & 0 & 0 & 0 & \frac{-1}{L_3} \\ 0 & \frac{-1}{C_1} & 0 & 0 & 0 & 0 \\ 0 & 0 & 0 & 0 & \frac{-1}{RC_0} & 0 \\ 0 & 0 & \frac{-1}{C_{Bt}} & 0 & 0 & \frac{1}{R_{Bt}C_{Bt}} \end{bmatrix}}_{A'} \begin{bmatrix} i_{L1}(t) \\ i_{L2}(t) \\ i_{L3}(t) \\ v_{C1}(t) \\ v_{C0}(t) \\ v_{CBt}(t) \end{bmatrix} + \underbrace{\begin{bmatrix} \frac{1}{L_1} \\ \frac{1}{L_2} \\ 0 \\ 0 \\ 0 \\ 0 \end{bmatrix}}_{B'} [V_{PV}],$$

$$\begin{bmatrix} i_{PV} \\ Vo \\ VBt \end{bmatrix} = \underbrace{\begin{bmatrix} 1 & 1 & 0 & 0 & 0 & 0 \\ 0 & 0 & 0 & 0 & 1 & 0 \\ 0 & 0 & 0 & 0 & 0 & 1 \end{bmatrix}}_{C'} \begin{bmatrix} i_{L1}(t) \\ i_{L2}(t) \\ i_{L3}(t) \\ v_{C1}(t) \\ v_{C0}(t) \\ v_{CBt}(t) \end{bmatrix} + \underbrace{\begin{bmatrix} 0 \\ 0 \\ 0 \\ 0 \\ 0 \\ 0 \end{bmatrix}}_{D'} [V_{PV}] \tag{35}$$

$$\begin{bmatrix} \dot{i}_{L1}(t) \\ \dot{i}_{L2}(t) \\ \dot{i}_{L3}(t) \\ \dot{v}_{C1}(t) \\ \dot{v}_{C0}(t) \\ \dot{v}_{CBt}(t) \end{bmatrix} = \underbrace{\begin{bmatrix} 0 & 0 & 0 & \frac{-1}{L_1} & 0 & 0 \\ 0 & 0 & 0 & \frac{-1}{L_2} & \frac{-1}{L_2} & 0 \\ 0 & 0 & 0 & 0 & \frac{1}{L_3} & \frac{-1}{L_3} \\ \frac{1}{C_1} & \frac{1}{C_1} & 0 & 0 & 0 & 0 \\ 0 & \frac{1}{C_0} & \frac{-1}{C_0} & 0 & \frac{-1}{RC_0} & 0 \\ 0 & 0 & \frac{-1}{C_{Bt}} & 0 & 0 & \frac{1}{R_{Bt}C_{Bt}} \end{bmatrix}}_{A''} \begin{bmatrix} i_{L1}(t) \\ i_{L2}(t) \\ i_{L3}(t) \\ v_{C1}(t) \\ v_{C0}(t) \\ v_{CBt}(t) \end{bmatrix} + \underbrace{\begin{bmatrix} 0 \\ 0 \\ 0 \\ 0 \\ 0 \\ 0 \end{bmatrix}}_{B''} [V_{PV}],$$

$$\begin{bmatrix} i_{PV} \\ Vo \\ VBt \end{bmatrix} = \underbrace{\begin{bmatrix} 0 & 0 & 0 & 0 & 0 & 0 \\ 0 & 0 & 0 & 0 & 1 & 0 \\ 0 & 0 & 0 & 0 & 0 & 1 \end{bmatrix}}_{C''} \begin{bmatrix} i_{L1}(t) \\ i_{L2}(t) \\ i_{L3}(t) \\ v_{C1}(t) \\ v_{C0}(t) \\ v_{CBt}(t) \end{bmatrix} + \underbrace{\begin{bmatrix} 0 \\ 0 \\ 0 \\ 0 \\ 0 \\ 0 \end{bmatrix}}_{D''} [V_{PV}] \tag{36}$$

$$\begin{bmatrix} \dot{i}_{L1}(t) \\ \dot{i}_{L2}(t) \\ \dot{i}_{L3}(t) \\ \dot{v}_{C1}(t) \\ \dot{v}_{C0}(t) \\ \dot{v}_{CBt}(t) \end{bmatrix} = \underbrace{\begin{bmatrix} 0 & 0 & 0 & \frac{-1}{L_1} & 0 & 0 \\ 0 & 0 & 0 & \frac{-1}{L_2} & \frac{-1}{L_2} & 0 \\ 0 & 0 & 0 & 0 & 0 & \frac{-1}{L_3} \\ \frac{1}{C_1} & \frac{1}{C_1} & 0 & 0 & 0 & 0 \\ 0 & \frac{1}{C_0} & 0 & 0 & \frac{-1}{RC_0} & 0 \\ 0 & 0 & \frac{1}{C_{Bt}} & 0 & 0 & \frac{-1}{R_{Bt}C_{Bt}} \end{bmatrix}}_{A'''} \begin{bmatrix} i_{L1}(t) \\ i_{L2}(t) \\ i_{L3}(t) \\ v_{C1}(t) \\ v_{C0}(t) \\ v_{CBt}(t) \end{bmatrix} + \underbrace{\begin{bmatrix} 0 \\ 0 \\ 0 \\ 0 \\ 0 \\ 0 \end{bmatrix}}_{B'''} [V_{PV}],$$

$$\begin{bmatrix} i_{PV} \\ Vo \\ VBt \end{bmatrix} = \underbrace{\begin{bmatrix} 0 & 0 & 0 & 0 & 0 & 0 \\ 0 & 0 & 0 & 0 & 1 & 0 \\ 0 & 0 & 0 & 0 & 0 & 1 \end{bmatrix}}_{C'''} \begin{bmatrix} i_{L1}(t) \\ i_{L2}(t) \\ i_{L3}(t) \\ v_{C1}(t) \\ v_{C0}(t) \\ v_{CBt}(t) \end{bmatrix} + \underbrace{\begin{bmatrix} 0 \\ 0 \\ 0 \\ 0 \\ 0 \\ 0 \end{bmatrix}}_{D'''} [V_{PV}] \tag{37}$$

$$\begin{bmatrix} \dot{i}_{L1}(t) \\ \dot{i}_{L2}(t) \\ \dot{i}_{L3}(t) \\ \dot{v}_{C1}(t) \\ \dot{v}_{C0}(t) \end{bmatrix} = \underbrace{\begin{bmatrix} 0 & 0 & 0 & 0 & 0 \\ 0 & 0 & 0 & \frac{1}{L_2} & 0 \\ 0 & 0 & 0 & 0 & 0 \\ 0 & \frac{-1}{C_1} & 0 & 0 & 0 \\ 0 & 0 & 0 & 0 & \frac{-1}{RC_0} \end{bmatrix}}_{A'} \begin{bmatrix} i_{L1}(t) \\ i_{L2}(t) \\ i_{L3}(t) \\ v_{C1}(t) \\ v_{C0}(t) \end{bmatrix} + \underbrace{\begin{bmatrix} \frac{1}{L_1} & 0 \\ \frac{1}{L_2} & 0 \\ 0 & \frac{1}{L_3} \\ 0 & 0 \\ 0 & 0 \end{bmatrix}}_{B'} \begin{bmatrix} V_{PV} \\ V_{Bt} \end{bmatrix},$$

$$\begin{bmatrix} i_{PV} \\ i_{Bt} \\ Vo \end{bmatrix} = \underbrace{\begin{bmatrix} 1 & 1 & 0 & 0 & 0 \\ 0 & 0 & 1 & 0 & 0 \\ 0 & 0 & 0 & 0 & 1 \end{bmatrix}}_{C'} \begin{bmatrix} i_{L1}(t) \\ i_{L2}(t) \\ i_{L3}(t) \\ v_{C1}(t) \\ v_{C0}(t) \end{bmatrix} + \underbrace{\begin{bmatrix} 0 & 0 \\ 0 & 0 \\ 0 & 0 \end{bmatrix}}_{D'} \begin{bmatrix} V_{PV} \\ V_{Bt} \end{bmatrix} \tag{39}$$

$$\begin{bmatrix} \dot{i}_{L1}(t) \\ \dot{i}_{L2}(t) \\ \dot{i}_{L3}(t) \\ \dot{v}_{C1}(t) \\ \dot{v}_{C0}(t) \end{bmatrix} = \underbrace{\begin{bmatrix} 0 & 0 & 0 & \frac{-1}{L_1} & 0 \\ 0 & 0 & 0 & \frac{-1}{L_2} & \frac{-1}{L_2} \\ 0 & 0 & 0 & 0 & \frac{-1}{L_3} \\ \frac{1}{C_1} & \frac{1}{C_1} & 0 & 0 & 0 \\ 0 & \frac{1}{C_0} & \frac{1}{C_0} & 0 & \frac{-1}{RC_0} \end{bmatrix}}_{A''} \begin{bmatrix} i_{L1}(t) \\ i_{L2}(t) \\ i_{L3}(t) \\ v_{C1}(t) \\ v_{C0}(t) \end{bmatrix} + \underbrace{\begin{bmatrix} 0 & 0 \\ 0 & 0 \\ 0 & \frac{1}{L_3} \\ 0 & 0 \\ 0 & 0 \end{bmatrix}}_{B''} \begin{bmatrix} V_{PV} \\ V_{Bt} \end{bmatrix},$$

$$\begin{bmatrix} i_{PV} \\ i_{Bt} \\ Vo \end{bmatrix} = \underbrace{\begin{bmatrix} 0 & 0 & 0 & 0 & 0 \\ 0 & 0 & 1 & 0 & 0 \\ 0 & 0 & 0 & 0 & 1 \end{bmatrix}}_{C''} \begin{bmatrix} i_{L1}(t) \\ i_{L2}(t) \\ i_{L3}(t) \\ v_{C1}(t) \\ v_{C0}(t) \end{bmatrix} + \underbrace{\begin{bmatrix} 0 & 0 \\ 0 & 0 \\ 0 & 0 \end{bmatrix}}_{D''} \begin{bmatrix} V_{PV} \\ V_{Bt} \end{bmatrix} \tag{40}$$

TABLE 2. Parameters of proposed system.

Input voltage V_{in}	12V (boost mode) and 30V (buck mode) for mode 1 (PV) 12V (Battery) mode 2, 18V (PV) for mode 3 18 V (PV) and 12 V (Battery) for mode 4
Output voltage V_o	24V (boost mode) and 18V (buck mode) for mode 1 24V for mode 2, 24V for mode 3, 24V for mode 4
Inductors L_1, L_2, L_3	1.4mH, 3.3mH, 0.75mH
Capacitors C_1, C_0	7.5µF, 18.75µF
Battery Voltage V_{Bt}	12V, 12 Ah
Switching frequency *fs*	20kHz

This error is compared with the fixed frequency sawtooth signal to determine the duty ratio. A 200W prototype is developed to demonstrate the feasibility of the proposed converter. The proposed prototype and experimental setup are shown in Fig. 6(c)-(d), respectively.

The control signals generated from Xilinx FPGA Spartan 6 are applied as gate pulses to power switches. The switching frequency of the gate pulses is 20 kHz. The components were chosen to allow a robust converter in the 25W to 200W output power range and guarantee operation in continuous conduction mode. The inductors L_1, L_2, and L_3 are designed to support the inductor currents in the selected power range. The designed components values of the proposed system are listed in Table 2. Various currents and voltages are sensed using the current sensor LA25-P and IC 7840 voltage sensors, respectively. A PV array with three series-connected 75W, 12V panels, 12V, 12 Ah sealed lead-acid batteries, and a resistive load are employed in the prototype.

A. MODE-1 (PV TO LOAD)

In this mode, the reference of the load voltage is defined as 24 V and load resistance $R = 40\Omega$. Fig. 7(a) shows the gate signal and the inductor currents. Identical gate signals are applied to S_1 and S_2 since both switches conduct synchronously. The average value of inductor currents I_{L1} and I_{L2} are 6.24A and 7.99A, respectively. With 12.5V input voltage, the buck-boost converter (Port-1 to Port-3) operates in boost mode with a duty cycle of 0.6 and gives the output voltage of 24V, as shown in Fig. 7(b).

The input and output current ripple is found to be 14% and 11%, respectively, which are slightly more than the assumed value of 10% in design calculation. Fig. 7(c) shows the gate signal and the inductor current when the input voltage is 30V, and a duty cycle is 0.4. The buck-boost converter operates in buck mode and gives 18V output to load. The obtained average value of inductor currents I_{L1} and I_{L2} are 750mA and 800mA, respectively. The PV voltage, current, load voltage and current are shown in Fig. 7(d). Input and output current ripple is found to be 12% and 10.2%, respectively. The observed efficiency of proposed converter through simulation and experiment is shown in Fig. 8(a). The maximum efficiency from the experimental results is about 93.6% and 82.7% during boost and buck mode, respectively. The dynamic response with the input voltage variation and load variation is shown in Fig. 8(b). As shown, the load voltage (Port-3) is maintained at 23.6V in spite of continuous fluctuations in PV voltage. In addition, the response of the converter when the load is varied from 25Ω to 50Ω and back from 50 Ω to 25 Ω is shown.

B. MODE-2 (BATTERY TO LOAD)

The battery provides energy to the load in the absence of PV power and regulates the load voltage. The maximum discharge current limit of the battery and the output voltage is defined as $I_{Bt(ref)} = 15$A and 24V, respectively. Fig. 9(a)-(b) shows the measured waveforms with $V_{Bt} = 12.6$V, and the

$$\begin{bmatrix} \dot{i}_{L1}(t) \\ \dot{i}_{L2}(t) \\ \dot{i}_{L3}(t) \\ \dot{v}_{C1}(t) \\ \dot{v}_{C0}(t) \end{bmatrix} = \underbrace{\begin{bmatrix} 0 & 0 & 0 & 0 & 0 \\ 0 & 0 & 0 & \frac{1}{L_2} & 0 \\ 0 & 0 & 0 & 0 & \frac{-1}{L_3} \\ 0 & \frac{-1}{C_1} & 0 & 0 & 0 \\ 0 & 0 & \frac{1}{C_0} & 0 & \frac{-1}{RC_0} \end{bmatrix}}_{A'''} \begin{bmatrix} i_{L1}(t) \\ i_{L2}(t) \\ i_{L3}(t) \\ v_{C1}(t) \\ v_{C0}(t) \end{bmatrix} + \underbrace{\begin{bmatrix} \frac{1}{L_1} & 0 \\ \frac{1}{L_2} & 0 \\ 0 & \frac{1}{L_3} \\ 0 & 0 \\ 0 & 0 \end{bmatrix}}_{B'''} \begin{bmatrix} V_{PV} \\ V_{Bt} \end{bmatrix},$$

$$\begin{bmatrix} i_{PV} \\ VBt \\ Vo \end{bmatrix} = \underbrace{\begin{bmatrix} 1 & 1 & 0 & 0 & 0 \\ 0 & 0 & 1 & 0 & 0 \\ 0 & 0 & 0 & 0 & 1 \end{bmatrix}}_{C'''} \begin{bmatrix} i_{L1}(t) \\ i_{L2}(t) \\ i_{L3}(t) \\ v_{C1}(t) \\ v_{C0}(t) \end{bmatrix} + \underbrace{\begin{bmatrix} 0 & 0 \\ 0 & 0 \\ 0 & 0 \end{bmatrix}}_{D'''} \begin{bmatrix} V_{PV} \\ V_{Bt} \end{bmatrix} \quad (41)$$

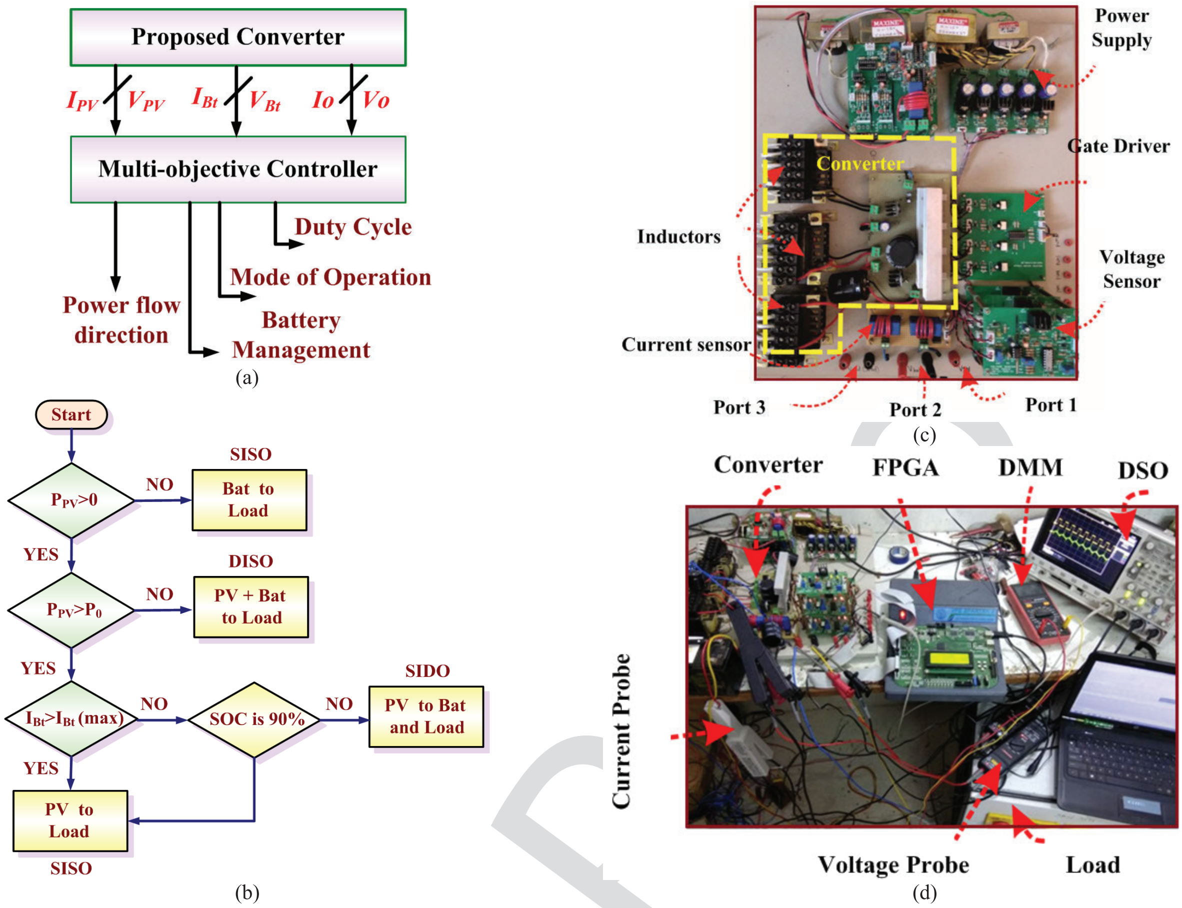

FIGURE 6. Control logic and hardware setup (a) System level control block diagram, (b) Flowchart for control logic of mode selection, (c) Prototype of the proposed multi-port converter, (d) Experimental prototype setup.

power of the battery is 96.4W. The gate signal to switch S_d and inductor current i_{L3} are shown in Fig. 9(a). The output voltage is controlled with S_d. Fig. 9(b) shows the regulated average battery current, $I_{Bt(avg)} = 7.65$A. It can be seen that the battery current in this mode has a positive value, which implies that the battery is discharging. The input and output current ripples are found as 11.7% and 11.1% respectively. The output voltage is regulated well. The dynamic response of the converter with the load variation is shown in Fig. 9(c). As shown, the load voltage (Port-3) is maintained at 24V.

C. MODE-3 (BATTERY CHARGING) AND MODE-4 (BATTERY DISCHARGING)

In this mode-3, PV provides energy to both load and battery. The battery charging current is limited to 1.5A, and the load (Port-3) voltage is defined as 24V. The Port-3 voltage is controlled by S_1 and S_2. The converter works in buck mode, and the battery voltage is regulated with S_C. The battery charging has been achieved with current mode control followed by voltage control.

Fig. 10(a) and Fig. 10(b) show the dynamic performance of the proposed converter in various modes of operation. After the converter is switched ON, the battery caters the load (Mode-2) until the MPPT tracks the maximum power as illustrated in Fig. 10(a). As the PV power increases, the current taken from the battery gradually reduces (Mode-4), i.e., both PV and battery ports share the output current. When it reaches maximum power, and PV power is more than the load consumption, the surplus PV power is fed to the battery for charging (Mode-3). When the load increases the charging current of the battery reduces to maintain the power balance. The positive average battery current $I_{Bt(avg)} = 1.2$A shows the charging characteristics. Also, the response of the converter when the input currents from port-1 and port-2 are continuously changing during mode-2 and mode-4 operations are shown in Fig. 10(a). The output voltage is regulated irrespective of the changes in input currents.

In Mode-4, both the PV and battery are supplying the load. The experimental results with $V_{PV} = 18$V, $V_{Bt} = 12.4$V and PV input power of 108W are illustrated in Fig. 10(b). The experiment has been carried out to show the response of the proposed converter for the sudden changes in parameters. When PV power is more, battery and load are catered by the PV source (Mode-3). When PV power suddenly reduces to zero, the battery is discharged and the current direction changes (Mode-2). In this condition, the battery provides energy to load. When PV power resumes, the current taken from the battery reduces (Mode-4). When the load reduces

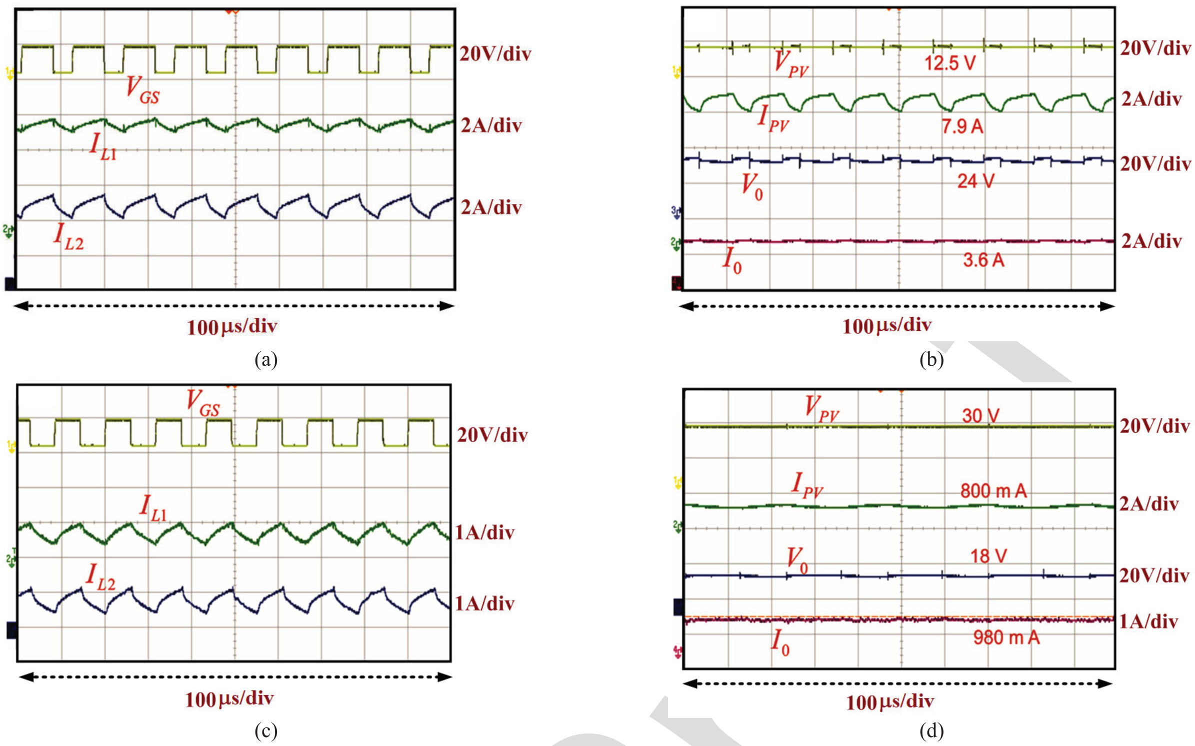

FIGURE 7. Hardware Result of mode-1 (a) Gate pulse, Inductor currents I_{L1} and I_{L2} (top to bottom) with duty cycle 60%, (b) PV voltage, PV current, Load voltage and Load current (top to bottom) with duty cycle 60%, (c) Gate pulse, Inductor currents I_{L1} and I_{L2} (top to bottom) with duty cycle 40%, (d) PV Voltage, PV current, Load voltage and Load current (top to bottom) with duty cycle 40%.

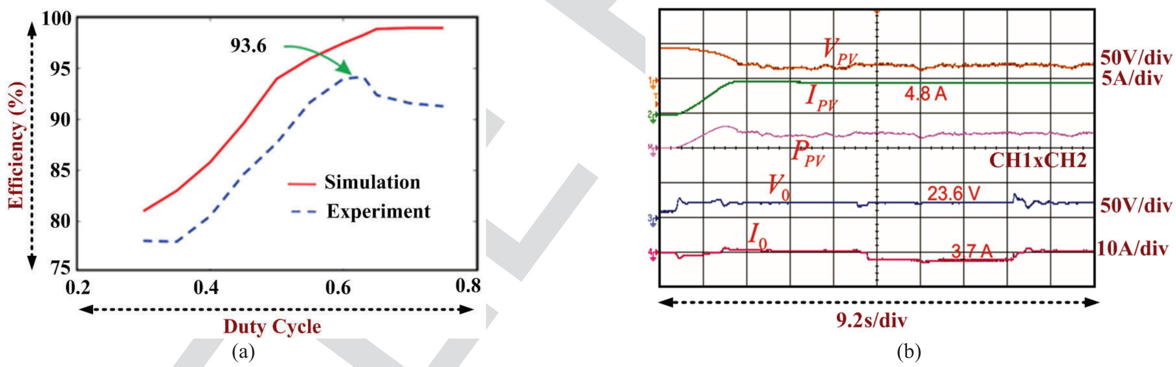

FIGURE 8. Efficiency and Dynamic Behavior (a) Efficiency versus duty cycle buck and boost operation. (plot through experimental data) (b) Dynamic response PV Voltage, current, load voltage and current (top to bottom).

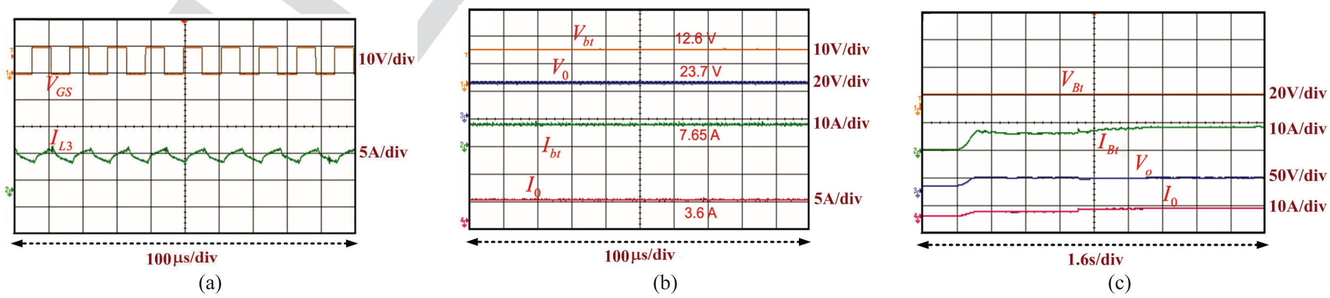

FIGURE 9. Hardware Result of mode-2 (a) Gate pulse, inductor current I_{L3} (top and bottom), (b) Battery voltage, load voltage, battery current and load current (top to bottom), (c) Dynamic response -Battery voltage, current, load voltage and current (top and bottom).

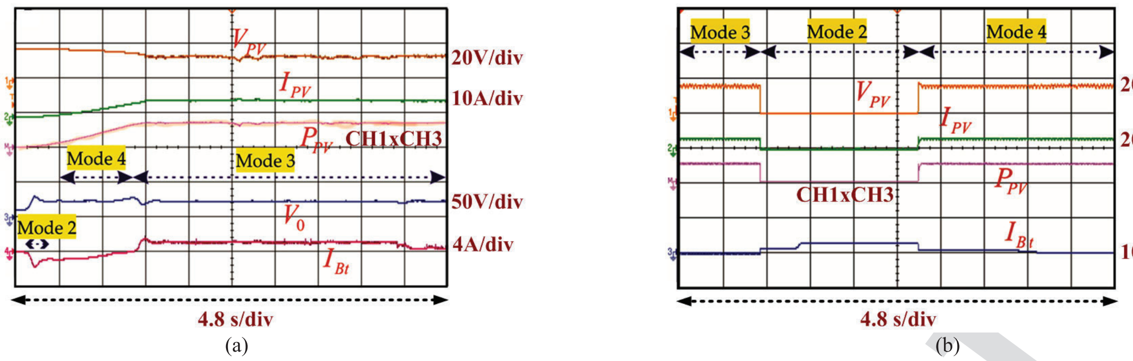

FIGURE 10. Hardware result of Mode 3 and Mode 4. (a) Dynamic behavior for P_{max} - PV Voltage, PV current, power, load voltage and battery current (top to bottom) (b) Dynamic behavior for 108W -PV voltage, PV current, power and battery current (top to bottom).

TABLE 3. Comparison of the proposed triple port converter with recently reported converters.

Converter	Number of Active switches	Number of diodes	Number of inductors	Number of capacitors	Switching frequency	Voltage Gain	Efficiency (%)	Reported power rating
[28]	4	2	1	1	10 kHz	High	91	-
[29]	3	4	2	3	40 kHz	High	92.7	200W
[30]	4	2	2	1	20 kHz	Medium	93.97	1kW
[31]	3	1	3	4	100 kHz	Medium	93.5	1.2kW
[32]	4	3	2	3	100 kHz	Low	96	400W
[33]	8	8	2, 2 coupled inductor	3	50 kHz	Medium	92 (expected)	-
[34]	3	3	1	2	20 kHz	High	93.5	120W
[35]	2	1	3	3	20 kHz	Low	92.74	100W
[36]	3	1	1	3	50 kHz	Medium	93.75	80W
Proposed converter	4	4	3	2	20 kHz	High	93.6	200W

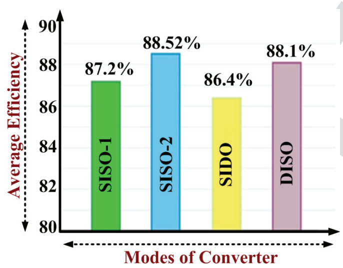

FIGURE 11. Experimentally observed average efficiencies for each mode.

the discharging current of the battery reduces to maintain the power balance. These responses indicate that the converter is controlled and offers stable operation. Several tests are conducted, and the graph of average efficiency for each mode is shown in Fig. 11 and the observed average efficiency for Mode 1 to Mode 4 is 87.2%, 88.52%, 86.4%, and 88.1%, respectively.

Table 3 shows a comparison of the NI-TP-BBB converter and other state-of-the-art TPCs in terms of components, voltage gain and efficiency. The converters [47], [53] and [82] have less efficiency and gain relatively. Thanks to the additional semiconductors which gives high step-up/step-down feature. Though the proposed triple port buck-boost converter has relatively more components, it provides high gain and relatively good efficiency when comparing with the TPC proposed in [83]. The power density (P.d) of the proposed converter is,

$$P.d = \frac{Power}{Volume} = \frac{200}{15 \times 21 \times 6} = 0.105W/cm^3 \quad (43)$$

AQ:5

VI. CONCLUSIONS

A new triple port converter with two unidirectional and one bi-directional port which integrate a photovoltaic module, battery and DC load is proposed. The proposed converter system provides a robust option for interfacing multiple renewable energy sources. The modes of operations with the characteristics waveform are discussed in detail. When PV is sufficient only to feed load, isolation of the battery from the main supply is achieved by using the switch control method. Also, the switch control method prevents the battery from overcharging and discharging. The proposed converter has positive high step-up/step-down output voltage (squared times of the voltage conversion ratio of classical buck-boost converter), and has a provision for step-up as well as step-down conversion with the simple control strategy. The higher voltage conversion ratio of the buck-boost converter is achieved by attaching an extra inductor at the drain of the switch of the buck-boost converter (the obtained structure is the hybrid version of buck and buck-boost converter). A constant DC bus voltage is maintained, and the PV array power characteristics follow the irradiance curve. Thus, the maximum power flow confirms from the PV array. The presented converter overcomes the drawback of the traditional buck-boost converter and verified by the obtained results. Experiment results are provided with dynamic performance, and it is verified that the proposed converter is an excellent choice for applications in both industrial and domestic applications.

REFERENCES

[1] F. Blaabjerg, Y. Yang, K. Ma, and X. Wang, "Power electronics–the key technology for renewable energy system integration," in *Proc. Int. Conf. Renew. Energy Res. Appl. (ICRERA)*, Palermo, Italy, Nov. 2015, pp. 1618–1626.

[2] M. Bhaskar, S. Padmanaban, and F. Blaabjerg, "A multistage DC-DC step-up self-balanced and magnetic component-free converter for photovoltaic applications: Hardware implementation," *Energies*, vol. 10, no. 5, p. 719, May 2017.

[3] S.-Y. Yu and A. Kwasinski, "Investigation of multiple-input converters bi-directional power flow characteristics," in *Proc. 28th Annu. IEEE Appl. Power Electron. Conf. Expo. (APEC)*, Mar. 2013, pp. 1095–1102.

[4] M. S. Bhaskar, M. Meraj, A. Iqbal, S. Padmanaban, P. K. Maroti, and R. Alammari, "High gain transformer-less double-duty-triple-mode DC/DC converter for DC microgrid," *IEEE Access*, vol. 7, pp. 36353–36370, 2019.

[5] M. S. Bhaskar, R. Alammari, M. Meraj, S. Padmanaban, and A. Iqbal, "A new triple-switch-triple-mode high step-up converter with wide range of duty cycle for DC microgrid applications," *IEEE Trans. Ind. Appl.*, vol. 55, no. 6, pp. 7425–7441, Nov. 2019.

[6] A. Iqbal, M. S. Bhaskar, M. Meraj, S. Padmanaban, and S. Rahman, "Closed-loop control and boundary for CCM and DCM of nonisolated inverting N× multilevel boost converter for high-voltage step-up applications," *IEEE Trans. Ind. Electron.*, vol. 67, no. 4, pp. 2863–2874, Apr. 2020.

[7] M. S. Bhaskar, M. Meraj, A. Iqbal, and S. Padmanaban, "Nonisolated symmetrical interleaved multilevel boost converter with reduction in voltage rating of capacitors for high-voltage microgrid applications," *IEEE Trans. Ind. Appl.*, vol. 55, no. 6, pp. 7410–7424, Nov. 2019.

[8] P. Sanjeevikumar, M. S. Bhaskar, P. Dhond, F. Blaabjerg, and M. Pecht, "Non-isolated sextuple output hybrid triad converter configurations for high step-up renewable energy applications," in *Advances in Power Systems and Energy Management*. Singapore: Springer, 2018, pp. 1–12.

[9] A. Kwasinski, "Identification of feasible topologies for multiple-input DC–DC converters," *IEEE Trans. Power Electron.*, vol. 24, no. 3, pp. 856–861, Mar. 2009.

[10] Y.-C. Liu and Y.-M. Chen, "A systematic approach to synthesizing multi-input DC–DC converters," *IEEE Trans. Power Electron.*, vol. 24, no. 1, pp. 116–127, Jan. 2009.

[11] M. Azizi, M. Mohamadian, and R. Beiranvand, "A new family of multi-input converters based on three switches leg," *IEEE Trans. Ind. Electron.*, vol. 63, no. 11, pp. 6812–6822, Nov. 2016.

[12] V. R. Teja, S. Srinivas, and M. K. Mishra, "A three port high gain non-isolated DC-DC converter for photovoltaic applications," in *Proc. IEEE Int. Conf. Ind. Technol. (ICIT)*, Taipei, Taiwan, Mar. 2016, pp. 251–256.

[13] H. Wu, J. Zhang, and Y. Xing, "A family of multiport Buck–Boost converters based on DC-link-inductors (DLIs)," *IEEE Trans. Power Electron.*, vol. 30, no. 2, pp. 735–746, Feb. 2015.

[14] J. Zhao, H. H. C. Iu, T. Fernando, L. An, and D. D.-C. Lu, "Design of a non-isolated single-switch three-port DC-DC converter for standalone PV-battery power system," in *Proc. IEEE Int. Symp. Circuits Syst. (ISCAS)*, Lisbon, Portugal, May 2015, pp. 2493–2496.

[15] M. R. Banaei and H. A. F. Bonab, "A novel structure for single-switch nonisolated transformerless Buck–Boost DC–DC converter," *IEEE Trans. Ind. Electron.*, vol. 64, no. 1, pp. 198–205, Jan. 2017.

[16] Y. Li, X. Ruan, D. Yang, F. Liu, and C. K. Tse, "Synthesis of multiple-input DC/DC converters," *IEEE Trans. Power Electron.*, vol. 25, no. 9, pp. 2372–2385, Sep. 2010.

[17] H. Wu, P. Xu, H. Hu, Z. Zhou, and Y. Xing, "Multiport converters based on integration of full-bridge and bidirectional DC–DC topologies for renewable generation systems," *IEEE Trans. Ind. Electron.*, vol. 61, no. 2, pp. 856–869, Feb. 2014.

[18] A. Ganjavi, H. Ghoreishy, and A. A. Ahmad, "A novel single-input dual-output three-level DC–DC converter," *IEEE Trans. Ind. Electron.*, vol. 65, no. 10, pp. 8101–8111, Oct. 2018.

[19] W. Li, C. Xu, H. Luo, Y. Hu, X. He, and C. Xia, "Decoupling-controlled triport composited DC/DC converter for multiple energy interface," *IEEE Trans. Ind. Electron.*, vol. 62, no. 7, pp. 4504–4513, Jul. 2015.

[20] Y.-E. Wu and P.-N. Chiu, "A high-efficiency isolated-type three-port bidirectional DC/DC converter for photovoltaic systems," *Energies*, vol. 10, no. 4, p. 434, Mar. 2017.

[21] M. S. Bhaskar, P. Sanjeevikumar, J. B. Holm-Nielsen, J. K. Pedersen, and Z. Leonowicz, "2L-2L converter: Switched inductor based high voltage step-up converter for fuel cell vehicular applications," in *Proc. IEEE Int. Conf. Environ. Electr. Eng. IEEE Ind. Commercial Power Syst. Eur. (EEEIC / I&CPS Europe)*, Genova, Italy, Jun. 2019, pp. 1–6.

[22] A. Iqbal, M. S. Bhaskar, M. Meraj, and S. Padmanaban, "DC-transformer modelling, analysis and comparison of the experimental investigation of a non-inverting and non-isolated Nx multilevel boost converter (Nx MBC) for low to high DC voltage applications," *IEEE Access*, vol. 6, pp. 70935–70951, 2018.

[23] M. S. Bhaskar, P. Sanjeevikumar, J. K. Pedersen, J. B. Holm-Nielsen, and Z. Leonowicz, "XL Converters- new series of high gain DC-DC converters for renewable energy conversion," in *Proc. IEEE Int. Conf. Environ. Electr. Eng. IEEE Ind. Commercial Power Syst. Eur. (EEEIC/I&CPS Europe)*, Genova, Italy, Jun. 2019, pp. 1–6.

[24] P. K. Maroti, S. Padmanaban, M. S. Bhaskar, M. Meraj, A. Iqbal, and R. Al-Ammari, "High gain three-state switching hybrid boost converter for DC microgrid applications," *IET Power Electron.*, vol. 12, no. 14, pp. 3656–3667, Aug. 2019.

[25] M. S. Bhaskar, R. Al-Ammari, M. Meraj, A. Iqbal, and S. Padmanaban, "Modified multilevel Buck–Boost converter with equal voltage across each capacitor: Analysis and experimental investigations," *IET Power Electron.*, vol. 12, no. 13, pp. 3318–3330, Nov. 2019.

[26] S. Miao, F. Wang, and X. Ma, "A new transformerless Buck–Boost converter with positive output voltage," *IEEE Trans. Ind. Electron.*, vol. 63, no. 5, pp. 2965–2975, May 2016.

[27] C.-W. Chen, C.-Y. Liao, K.-H. Chen, and Y.-M. Chen, "Modeling and controller design of a semiisolated multiinput converter for a hybrid PV/wind power charger system," *IEEE Trans. Power Electron.*, vol. 30, no. 9, pp. 4843–4853, Sep. 2015.

[28] L. Kumar and S. Jain, "Multiple-input DC/DC converter topology for hybrid energy system," *IET Power Electron.*, vol. 6, no. 8, pp. 1483–1501, Sep. 2013.

[29] M. Kumar, Y. N. Babu, D. Pullaguram, and S. Mishra, "A high voltage gain non-isolated modified three-port DC/DC converter based on integrated Boost-Cuk topology," in *Proc. IEEE PES Asia–Pacific Power Energy Eng. Conf. (APPEEC)*, Bengaluru, India, Nov. 2017, pp. 1–6.

[30] F. Akar, Y. Tavlasoglu, E. Ugur, B. Vural, and I. Aksoy, "A bidirectional non-isolated multi-input DC–DC converter for hybrid energy storage systems in electric vehicles," *IEEE Trans. Veh. Tech.*, vol. 65, no. 10, pp. 7944–7955, Oct. 2016.

[31] H. Zhu, D. Zhang, B. Zhang, and Z. Zhou, "A non-isolated three-port DC–DC converter and three-domain control method for PV-battery power systems," *IEEE Trans. Ind. Electron.*, vol. 62, no. 8, pp. 4937–4947, Aug. 2015.

[32] Z. Zhou, H. Wu, X. Ma, and Y. Xing, "A non-isolated three-port converter for stand-alone renewable power system," in *Proc. IECON-38th Annu. Conf. IEEE Ind. Electron. Soc.*, Montreal, QC, Canada, Oct. 2012, pp. 3352–3357.

[33] S. Hosseini, Z. Saadatizadeh, and P. Herís, "A new multiport non-isolated bidirectional DC/DC converter with zero voltage switching and free ripple input currents," in *Proc. IEEE 10th Int. Conf. Electr. Electron. Eng. (ELECO)*, Bursa, Turkey, Nov./Dec. 2017, pp. 279–284.

[34] P. Zhang, Y. Chen, and Y. Kang, "Nonisolated wide operation range three-port converters with variable structures," *IEEE J. Emerg. Sel. Topics Power Electron.*, vol. 5, no. 2, pp. 854–869, Jun. 2017.

[35] C. Balaji, N. Chellammal, and B. Nallamothu, "Non-isolated unidirectional three-port Cuk-Cuk converter for fuel cell/solar PV systems," *J. Power Electron.*, vol. 19, no. 5, pp. 1278–1288, Sep. 2019.

[36] M. Al-Soeidat, H. Aljarajreh, H. Khawaldeh, D. D.-C. Lu, and J. G. Zhu, "A reconfigurable three-port DC-DC converter for integrated PV-battery system," *IEEE J. Emerg. Sel. Topics Power Electron.*, early access, Sep. 16, 2019, doi: 10.1109/JESTPE.2019.2941595.

BALAJI CHANDRASEKAR (Graduate Student Member, IEEE) was born in Arakkonam, India. He received the B.E. degree in electrical and electronics engineering from the IFET College of Engineering, Villupuram, the M.E. degree in control and instrumentation engineering from the College of Engineering, Guindy, Anna University, India, and the D.Phil. degree in power electronics from the Department of Electrical and Electronics Engineering, SRM Institute of Science and Technology, Chennai. He is currently an Assistant Professor with the Department of Electrical and Electronics Engineering, SRMIST. He has authored more than 15 technical papers published in journals and conference proceedings. He has also authored a book titled *Measurement and Instrumentation* for undergraduate students. His current research interests include multi-port power electronic converters and renewable energy systems. He is a member of the Institution of Engineers, India, and Indian Society for Technical Education, India.

CHELLAMMAL NALLAPERUMAL received the M.Sc. degree in engineering in electrical drives and automation from Tashkent State Technical University, Tashkent, and the Ph.D. degree in power electronics from the Faculty of Engineering, SRM Institute of Science and Technology, India. She is currently an Associate Professor with the SRM Institute of Science and Technology. She has authored more than 30 peer-reviewed papers published in journals and conference proceedings. Her main areas of expertise are modeling of power electronic converters and drives, grid integration of renewable energy resources, and design of controllers.

SANJEEVIKUMAR PADMANABAN (Senior Member, IEEE) received the bachelor's degree in electrical engineering from the University of Madras, Chennai, India, in 2002, the master's degree (Hons.) in electrical engineering from Pondicherry University, Puducherry, India, in 2006, and the Ph.D. degree in electrical engineering from the University of Bologna, Bologna, Italy, in 2012. He was an Associate Professor with VIT University, from 2012 to 2013. In 2013, he joined the National Institute of Technology, India, as a Faculty Member. In 2014, he was invited as a Visiting Researcher at the Department of Electrical Engineering, Qatar University, Doha, Qatar, funded by the Qatar National Research Foundation (Government of Qatar). He continued his research activities with the Dublin Institute of Technology, Dublin, Ireland, in 2014. He was an Associate Professor with the Department of Electrical and Electronics Engineering, University of Johannesburg, Johannesburg, South Africa, from 2016 to 2018. Since 2018, he has been a Faculty Member with the Department of Energy Technology, Aalborg University, Esbjerg, Denmark. He has authored more than 300 scientific articles.

Dr. Padmanaban is a Fellow of the Institution of Engineers, India, the Institution of Electronics and Telecommunication Engineers, India, and the Institution of Engineering and Technology, U.K. He was a recipient of the Best Paper cum Most Excellence Research Paper Award from IET-SEISCON'13, IET-CEAT'16, IEEE-EECSI'19, IEEE-CENCON'19 and five best paper awards from ETAEERE'16 sponsored Lecture Notes in Electrical Engineering, Springer book. He is an Editor/Associate Editor/Editorial Board of refereed journals, in particular the IEEE SYSTEMS JOURNAL, IEEE TRANSACTIONS ON INDUSTRY APPLICATIONS, IEEE ACCESS, *IET Power Electronics*, and *International Transaction on Electrical Energy Systems,* Wiley, and the Subject Editor of the *IET Renewable Power Generation*, *IET Generation, Transmission and Distribution*, and *FACTS* journal, Canada.

MAHAJAN SAGAR BHASKAR (Member, IEEE) received the bachelor's degree in electronics and telecommunication engineering from the University of Mumbai, Mumbai, India, in 2011, the master's degree in power electronics and drives from the Vellore Institute of Technology, VIT University, India, in 2014, and the Ph.D. degree in electrical and electronic engineering from the University of Johannesburg, South Africa, in 2019. He was a Postdoctoral Researcher with his Ph.D. tutor with the Department of Energy Technology, Aalborg University, Esbjerg, Denmark, in 2019. He worked as a Researcher Assistant at the Department of Electrical Engineering, Qatar University, Doha, Qatar, from 2018 to 2019. He worked as a Research Student with the Power Quality Research Group, Department of Electrical Power Engineering, Universiti Tenaga Nasional (UNITEN), Kuala Lumpur, Malaysia, from August 2017 to September 2017. He is currently with the Renewable Energy Lab, Department of Communications and Networks Engineering, College of Engineering, Prince Sultan University, Riyadh, Saudi Arabia. He has authored 100 plus scientific articles particular reference to DC/DC and DC/AC converter, and high gain converter. He is a member of the IEEE Industrial Electronics, Power Electronics, Industrial Application, and Power and Energy, Robotics and Automation, Vehicular Technology Societies, Young Professionals, and various IEEE Councils and Technical Communities. He received the Best Paper Research Paper Awards from IEEE-CENCON'19, IEEE-ICCPCT'14, IET-CEAT'16, and ETAEERE'16 sponsored Lecture note in Electrical Engineering, Springer book series. He received the IEEE ACCESS award Reviewer of Month, in January 2019, for his valuable and thorough feedback on manuscripts, and for his quick turnaround on reviews. He is a reviewer member of various international journals and conferences including IEEE and IET.

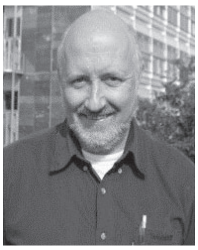

JENS BO HOLM-NIELSEN received the M.Sc. degree in agricultural systems, crops and soil science from the KVL, Royal Veterinary and Agricultural University, Copenhagen, Denmark, in 1980, and the Ph.D. degree in process analytical technologies for biogas systems from Aalborg University, Esbjerg, Denmark, in 2008. He is currently with the Department of Energy Technology, Aalborg University, and the Head of the Esbjerg Energy Section. He is the Head of the research group at the Center for Bioenergy and Green Engineering established, in 2009. He has vast experience in the field of biorefinery concepts and biogas production–anaerobic digestion. He has implemented projects of bioenergy systems in Denmark with provinces and European states. He was the Technical Advisor for many industries in this field. He has executed many large-scale European Union and United Nations projects in research aspects of bioenergy, biorefinery processes, and the full chain of biogas and green engineering. He has authored more than 300 scientific articles. His current research interests include renewable energy, sustainability, and green jobs for all. He was a member on the invitation with various capacities in the committee for over 500 various international conferences and organizer of international conferences, workshops, and training programs in Europe, Central Asia, and China.

ZBIGNIEW LEONOWICZ (Senior Member, IEEE) received the M.Sc., Ph.D., and Dr.Sci. degrees in electrical engineering from the Wroclaw University of Science and Technology, Wroclaw, Poland, and the Habilitate Doctorate degree from the Bialystok University of Technology, Bialystok, Poland in 1997, 2001, and 2012, respectively. Since 1997, he has been with the Department of Electrical Engineering, Wroclaw University of Science and Technology, where he is currently an Associate Professor. His current research interests include power quality, control and protection of power systems, renewables, industrial ecology, and applications of advanced signal processing methods in power systems.

SAMSON O. MASEBINU received the bachelor's degree in mechanical engineering from the Federal University of Technology, Akure, Nigeria, in 2011, the master's degree in chemical engineering technology from the University of Johannesburg, Gauteng, South Africa, in 2015, and the Ph.D. degree in mechanical engineering from the University of Johannesburg, in 2019. He undertook his postdoctoral research fellowship at the University of Johannesburg. He is currently a Visiting Researcher, under the DANIDA funding with the Department of Energy Technology, Aalborg University, Esbjerg, Denmark. He has won several awards among which are the most outstanding masters research in the Faculty of Engineering and the Built Environment, University of Johannesburg, First position in interfaculty 3-mins Ph.D. thesis competition and postdoctoral award of excellence for academic achievement at the University of Johannesburg. He has worked on several projects, mainly in the field of renewable energy and environmental sustainability. He currently works as an Engineer and a Research Lead for the Process and Energy Engineering Unit, Process, Energy and Environmental Technology Station, University of Johannesburg. He has authored more than 35 scientific articles and reports. He is a registered member of the Engineering Council of South Africa.